[AMERICAN JOURNAL OF SCIENCE, VOL. 294, MAY, 1994, P. 529–592]

American Journal of Science

MAY 1994

A COUPLED MODEL FOR TRANSPORT OF MULTIPLE CHEMICAL SPECIES AND KINETIC PRECIPITATION/DISSOLUTION REACTIONS WITH APPLICATION TO REACTIVE FLOW IN SINGLE PHASE HYDROTHERMAL SYSTEMS

CARL I. STEEFEL* and ANTONIO C. LASAGA
Department of Geology and Geophysics,
Yale University, P.O. Box 208109,
New Haven, Connecticut 06520-8109

ABSTRACT. The essential features of a numerical model for computing coupled multi-component chemical reactions, multi-species chemical transport, hydrodynamic flow, and heat transfer are described. The model employs a new algorithm which solves simultaneously for multi-component reactions and solute transport in one and two dimensions and which uses kinetic formulations for mineral dissolution and precipitation reactions, making the *a priori* assumption of equilibrium between water and minerals unnecessary. This feature is then used to assess the validity of the local equilibrium approximation in single phase hydrothermal systems. The code is also used to examine the problem of reaction-induced porosity and permeability changes in a fractured hydrothermal system.

The numerical calculations indicate that significant disequilibrium with respect to silicate phases is likely in thermal boundary layers developed at low temperature, permeable interfaces (for example, at the seafloor). Disequilibrium is less pronounced in the thermal boundary layers of systems with impermeable upper surfaces because of the local reduction in flow velocities near the boundary. The calculations show that the extent of disequilibrium in thermal boundary layers formed in fractured rock depends on the fracture spacing (or fracture aperture) and on the flow rate, which affects *both* the rate of solute transport and the thickness of the thermal boundary layer. In the high temperature, nearly isothermal inner portions of high Rayleigh number convection cells, disequilibrium is possible only where very rapid flow and/or widely spaced fractures occur. In systems where the flow is sufficiently slow that linear temperature gradients occur, disequilibrium with respect to silicate phases is likely only in the case where the fractures are extremely widely spaced. The calculations also suggest that the presence or absence of metastable phases (for example, amorphous silica) may be used to estimate permeabilities in paleo-hydrothermal systems if fracture spacings can be determined.

* Present Address: Battelle, Pacific Northwest Laboratories, MS K3-61, P.O. Box 999, Richland, Washington 99352

Two dimensional calculations of reactive flow in a model single phase geothermal field with a porosity-permeability relationship such as that observed in the contact aureole of the Skaergaard intrusion in Greenland (Manning and Bird, 1991) suggest that the local equilibrium approximation is fully justified in such a system. The same model geothermal system and porosity-permeability relationship have also been used to study the effects of reaction-induced porosity and permeability change on the character of the convective regime. The calculations indicate that the rates of permeability change may be sufficiently rapid that the convection cell never attains a hydrodynamic or thermal steady state. Permeability reduction, which tends to occur where upwelling fluids cool, causes the plume to become increasingly diffuse with time because the ascending fluids diverge around the cemented zone. Permeability enhancement, which most commonly occurs where fluids move up temperature, can result in an instability which causes channeling of flow. These effects do not depend on any particular concentration boundary condition but rather are the natural consequence of imposed thermal gradients in hydrothermal systems.

INTRODUCTION

A major objective of the current research on water-rock interaction is to develop a more quantitative basis for its study. One of the most important aspects of developing a quantitative approach to water-rock interaction is the treatment of geochemical reactions and transport of heat, fluid, and solutes as coupled phenomena. Most of the important examples of water-rock interaction take place in open systems, where ultimately the rates at which the rock is altered depend on the rates of transport (Phillips, 1991; Lichtner, 1993). A quantitative prediction of the rates of reaction, therefore, requires that solute transport, and, where appropriate, heat and fluid transport, be explicitly considered. While a rigorously quantitative treatment of water-rock interaction is many years away, we would argue that it is important to begin to understand how some of the various dynamical processes taking place in the rock couple to each other, even if the analysis is carried out on somewhat simplified variants of complicated geological settings. In this paper, we present a preliminary attempt at a quantitative, coupled approach to the problem of water-rock interaction. We describe the essential features of a numerical model for coupled multi-component reaction, solute transport, heat transfer, and fluid flow and apply it to several important problems relating to reactive hydrothermal systems.

A number of excellent studies have examined the problem of hydrodynamic flow and heat transfer in various geological settings (Donaldson, 1962; Elder, 1965, 1967a,b, 1981; Combarnous and Bories, 1975; Ribando and Torrance, 1976; Norton and Knight, 1977; Cathles, 1977, 1981, 1983; Cheng, 1978; Norton, 1978, 1984; Norton and Cathles, 1979; Norton and Taylor, 1979; Garven and Freeze, 1984a,b; Bethke, 1985, 1986; Garven, 1989; Phillips, 1991; Lowell, 1991; Lowell, Van Cappellen, and Germanovich, 1993). A separate line of research has focused on developing and applying quantitative models for irreversible

chemical reactions in multi-component and multi-mineralic systems, beginning with the seminal studies by Helgeson (1968) and Helgeson, Garrels, and MacKenzie (1969) of the irreversible weathering of granite. These early studies were followed by the application of similar models to a number of different geological environments (Brimhall, 1980; Reed, 1982, 1983; Brimhall and Ghiorso, 1983; Sverjensky, 1984; Bowers and Taylor, 1985). The logical next step in the development of quantitative models is to couple chemical reactions with mass transport (Rubin, 1983; Miller and Benson, 1983; Walsh and others, 1984; Lasaga, 1984; Lichtner, 1985, 1988, 1992; Bryant, Schechter, and Lake, 1987; Schechter, Bryant, and Lake, 1987; Kirkner and Reeves, 1988; Ague and Brimhall, 1989; Liu and Narasimhan, 1989a,b; Novak, Schechter, and Lake, 1989; Steefel and Lasaga, 1990, 1992; Steefel and Van Cappellen, 1990; Yeh and Tripathi, 1991; Wells and Ghiorso, 1991; Phillips, 1991; Lichtner and Biino, 1992; Steefel, 1992; Sevougian, Schechter, and Lake, 1993).

Most of the studies of reactive transport in geological systems have made use of the local equilibrium approximation. The assumption of local equilibrium has long been one of the most fundamental tenets of hydrothermal and metamorphic geochemistry and petrology. With the rapidly accumulating database on mineral-fluid reaction rates, however, it is possible to begin to assess the validity of the local equilibrium approximation (Bahr and Rubin, 1987; Knapp, 1989; Steefel and Van Cappellen, 1990; Lasaga and Rye, 1993). Such an assessment requires that the geochemical reaction rates be linked to the appropriate transport rates in the open system of interest. It is also surprising how few studies have investigated how reactions and fluid flow couple through reaction-induced porosity and permeability changes, despite the potentially enormous geological significance of these effects (Ortoleva and others, 1987; Hoefner and Fogler, 1988; Sanford and Konikow, 1989; Steefel and Lasaga, 1990; Chen and others, 1990).

These are just two of the important problems that need to be addressed via reaction-transport modeling. The treatment of chemical reaction and fluid flow as coupled processes, however, has not been considered feasible because of the sheer size and to some extent the complexity of the problem. Analytical solutions to the reaction-transport equation (Ogata and Banks, 1961; Bear, 1972, 1979; Fletcher and Hoffman, 1974; Bickle and McKenzie, 1988; Lassey and Blattner, 1988; Lichtner, 1988; Lasaga, 1989; Phillips, 1991) offer some important insights into the underlying dynamics of the coupled system, but because they are restricted to one-dimensional systems with constant flow fields and to a single chemical component, they cannot describe the full range of complex phenomena that emerge when multi-component, multi-dimensional transport and reaction are considered. In their full form, the governing differential equations for coupled reaction and transport are nonlinear and therefore must be solved using numerical methods. The dramatic increase in computational power which has become available in the last few years at relatively low cost has made the numerical treatment

of the problem of multi-dimensional and multi-component reaction and transport feasible for the first time. We make the further prediction that the availability of massively parallel computers in the future will eventually make the multi-dimensional reaction-transport problem routine.

The paper begins with a discussion of the features of the numerical approach presented here which are noteworthy, although individually they are not necessarily unique to this particular code. One important feature is the use of a finite difference formulation for computing coupled reaction and transport for multi-component and multi-mineralic systems. The finite difference method, although computationally more intensive than the simpler reaction path models, allows for modeling of the entire range of both transient and steady-state phenomena, including advective, dispersive, and diffusive transport or any combination of these. A second important feature is the use of a kinetic formulation for all the mineral-water reactions. The approach described is the only one we are aware of, along with the recent study of Sevougian, Schechter, and Lake (1993), which combines a finite difference approach and kinetically-controlled, multi-component mineral-water reactions. The discussion of these features is followed by a description of the mathematical and numerical formulations used in the code. The chief innovation is the use of a *global implicit* or *one-step* method to solve the combined reaction and solute transport terms (in other words, the reaction and solute transport terms are solved simultaneously rather than in sequence). Another notable feature is the use of basis switching (rewriting the reactions locally in terms of the dominant aqueous species) which may improve both the convergence properties and the robustness of the numerical calculations. Finally, as applications of the reaction-transport model, we attempt to assess the validity of the local equilibrium approximation in hydrothermal systems, and we examine the problem of reaction-induced permeability change in a hydrothermal convection cell.

A FINITE DIFFERENCE MODEL

The approach to modeling reactive flow adopted here is to use numerical methods based on the finite difference method. The finite difference method, like the finite element method, breaks the domain of interest up into a series of discrete blocks or elements. The methods are applied to problems where an analytical solution to the governing partial differential equation is not available. A numerical solution is obtained instead by solving N algebraic equation, where N is the number of blocks or elements used to discretize the spatial domain. The accuracy with which the governing set of partial differential equations can be solved, therefore, depends on the number of blocks or elements used. In a multi-component chemical system, we also have to consider M independent components, so that in practice the minimum number of equations to be solved at every time step is $N \times M$. This is why finite difference methods have not been widely used. The finite difference (or element)

method, however, does have the advantage that it is a perfectly general approach applicable to all forms of solute transport (advection, dispersion, and diffusion or any combination of these) and to both steady-state and transient problems. In addition, the method can be extended (at least in theory) to two or three dimensions, an essential capability for modeling many hydrogeochemical phenomena.

The first step in formulating the problem in terms of finite differences is to define a *representative elementary volume* or REV which is large enough that one can define a mean property (for example, permeability, reactive surface area, et cetera) for that region and yet small enough that one can resolve the features of interest. Because of the computational cost of using fine grids in the case of the multi-component reaction and transport, the second condition is difficult to achieve for many systems at the present time. In the classical finite difference approach (Lapidus and Pinder, 1982; Marsily, 1986), one gives to a mathematical point in space the mean properties of the REV surrounding that point. In the slightly different integrated finite difference method, the properties are averaged instead over the boundaries of the volume (Narasimhan and Witherspoon, 1976; Marsily, 1986). The basic concept, however, is the same: by breaking the domain of interest up into a number of discrete volumes, the spatial derivatives in the governing equations can be approximated as differences (thus the name). If the time derivative is also approximated as a difference, then the partial differential equations are converted into a set of simultaneous algebraic equations.

KINETIC VERSUS EQUILIBRIUM MODELS

An important consideration in constructing a model for coupled reaction and transport is whether to assume that the fluid phase is in local equilibrium with the minerals in the rock or whether to use a kinetic formulation. There can be some computational advantages to assuming equilibrium. In particular, the assumption of equilibrium among the various aqueous species allows one to reduce significantly the number of actual chemical unknowns in the system (Reed, 1982; Lichtner, 1985; Kirkner and Reeves, 1988). The key question is what kind of errors the assumption of local equilibrium introduces into the calculations. In the case of reactions taking place between aqueous species (homogeneous reactions), most of them are much more rapid than the normal rates of transport due to fluid flow. This may not be true for various oxidation-reduction reactions at low temperature (Ohmoto and Lasaga, 1982). A number of mineral-water reactions, however, are extremely slow at low temperature (Rimstidt and Barnes, 1980; Lasaga, 1984; Nagy, Blum, and Lasaga, 1991), and the assumption of local equilibrium may not be justified (Steefel and Van Cappellen, 1990; Nagy and others, 1990).

A second argument often cited in favor of the assumption of local equilibrium is that we know very little about mineral-water reaction rates

and even less about mineral reactive surface areas in natural systems. This is true enough, but it is important to point out that this is an inherent complexity in nature and *not* an artifact of the kinetic model. A local equilibrium model only avoids this problem by choosing reaction rates that are much faster than the rates of transport. One does not, therefore, completely avoid the problems associated with our lack of knowledge of kinetics.

Local equilibrium is, of course, a limiting condition in which the rates of reaction are much more rapid than the rates of solute transport (Thompson, 1959; Helgeson, 1979; Bahr and Rubin, 1987; Knapp, 1989). This implies that a kinetic as opposed to equilibrium formulation is always the more general approach in describing mineral-water reactions. It is only with a kinetic model that one can attempt to assess the validity of the local equilibrium approximation. One expects that a "kinetic" model should produce "equilibrium" behavior under the right set of circumstances.

We have used a kinetic formulation for all the mineral-water reactions included in the present code. Equilibrium is assumed among the various aqueous species present, although this requirement needs to be relaxed in future developments in order to model low-temperature oxidation-reduction reactions in natural waters. The one and two-dimensional simulations of reactive flow in hydrothermal systems presented below are used to attempt to estimate the conditions where the local equilibrium approximation is likely to be valid.

MATHEMATICAL FORMULATION

Conservation of solute mass.—A partial differential equation describing the conservation of solute mass in the aqueous phase of a system that includes both transport and reaction in saturated porous media can be written

$$\frac{\partial(\phi C_i)}{\partial t} + \nabla \cdot (\mathbf{J}_{disp} + \mathbf{J}_{adv} + \mathbf{J}_{diff}) = R_i \quad (i = 1, 2, \ldots, N_{tot}), \qquad (1)$$

where C_i is the mass concentration of some species in solution (in units of moles per unit volume solution), N_{tot} is the total number of aqueous species, $\mathbf{J}_{disp}$, $\mathbf{J}_{diff}$, and $\mathbf{J}_{adv}$ are the dispersive, diffusive, and advective fluxes respectively (all in units of moles per unit area rock per unit time), and R_i (in units of moles per unit volume rock per unit time) is the total reaction rate of species i in solution. Note that the porosity, ϕ, is imbedded in both the flux terms and the reaction terms as described below. If the system is not isothermal, then the concentration can be written in terms of the fluid density, ρ_f, and the molality, m_i,

$$C_i = \rho_f m_i. \qquad (2)$$

The reaction term R_i can be divided into dissolution-precipitation (heterogeneous) reactions, R_i^{min}, and aqueous (homogeneous) reactions, R_i^{aq}, such that

$$R_i = R_i^{min} + R_i^{aq}. \tag{3}$$

if sorption reactions are neglected. The reaction rate is written here in terms of a unit volume of rock but could be written equivalently per unit volume of fluid if it were then multiplied by the porosity, ϕ.

The advective flux is given by

$$\mathbf{J}_{adv} = \mathbf{u}C_i, \tag{4}$$

where $\mathbf{u}$ is the Darcy fluid flux. The Darcy flux is related to the average linear velocity (or "true velocity") of the fluid, $\mathbf{v}$, by

$$\mathbf{u} = \phi\mathbf{v}. \tag{5}$$

The dispersive flux is given by (Marsily, 1986)

$$\mathbf{J}_{disp} = -\mathbf{D}_\mathbf{h}\nabla C_i, \tag{6}$$

where $\mathbf{D}$ is the mechanical or kinematic dispersion tensor. The dispersion is assumed to be second order and to have as its principal direction the velocity vector of the flow. The dispersion tensor consists of a longitudinal dispersion coefficient, D_L, in the direction of the flow and a tranverse dispersion coefficient, D_T, perpendicular to the flow direction. The dispersion coefficients are usually assumed to depend on the flow velocities according to

$$D_L = \alpha_L|u| \tag{7}$$

and

$$D_T = \alpha_T|u| \tag{8}$$

where $|u|$ is the absolute value of the Darcy flux, and α_L and α_T are the longitudinal and transverse dispersivities respectively. If we choose a coordinate system such that one of the axes corresponds to the direction of flow, then the dispersion tensor for a two dimensional system becomes

$$\mathbf{D}_\mathbf{h} = \begin{bmatrix} \alpha_L|u| & 0 \\ 0 & \alpha_T|u| \end{bmatrix}. \tag{9}$$

Note that off-diagonal terms arise when one of the coordinate axes is not parallel to the flow. The diffusive flux is given by

$$\mathbf{J}_{diff} = -D^*\nabla C_i, \tag{10}$$

where D^* is the molecular diffusion coefficient in porous media (Marsily, 1986). For the sake of compactness, we can combine the hydrodynamic

dispersion coefficient and the molecular diffusion coefficient into a single dispersion/diffusion coefficient given by (Bear, 1979)

$$\mathbf{D} = \mathbf{D_h} + D^*. \tag{11}$$

The heterogeneous reaction term R_i^{min} can be written more explicitly as the sum of all the individual mineral-water reactions that affect the concentration of the ith species

$$R_i^{min} = -\sum_{m=1}^{N_m} \nu_{im} r_m, \tag{12}$$

where r_m is the rate of precipitation or dissolution of mineral m per unit volume rock, ν_{im} is the number of moles of i in mineral m, and N_m is the number of minerals present in the rock. By convention, r_m is taken as positive for precipitation and negative for dissolution.

Eq (1) provides a general formulation for the conservation of solute mass which makes no assumptions of chemical equilibrium. It is possible to reduce the number of *independent* concentrations (the number that actually need to be solved), if we assume that the aqueous species are in chemical equilibrium. Mathematically, this means that in a system containing N_{tot} aqueous species, the number of independent chemical components in the system N_c is reduced from the total number of species by the N_x linearly independent chemical reactions between them (for further discussion, see Hooyman, 1961; Aris, 1965; Bowen, 1968; Van Zeggeren and Storey, 1970; Parkhurst, Thorstenson, and Plummer, 1980; Reed, 1982; Lichtner, 1985; Kirkner and Reeves, 1988). This leads to a natural partitioning of the system into N_c *primary* species, designated here as C_j, and the N_x *secondary* species, referred to as X_i (Reed, 1982; Lichtner, 1985; Kirkner and Reeves, 1988). The reversible chemical reactions between the primary and secondary species take the form

$$A_i \rightleftharpoons \sum_{j=1}^{N_c} \nu_{ij} A_j \qquad (i = 1, \ldots, N_x), \tag{13}$$

where the A_j and the A_i are the chemical formulas of the primary and secondary species respectively and ν_{ij} is the number of moles of primary species j in one mole of secondary species i. It should be noted here that the partitioning between the primary and secondary species is not unique, that is, we can write the chemical reactions in more than one way. The reversible reactions provide an algebraic link between the primary and secondary species via the law of mass action for each reaction

$$X_i = K_i^{-1} \gamma_i^{-1} \prod_{j=1}^{N_c} (\gamma_j C_j)^{\nu_{ij}} \qquad (i = 1, \ldots, N_x), \tag{14}$$

where the K_i are the equilibrium constants of the reaction given in eq (13), written here as the destruction of one mole of the secondary species. Given this partition between primary and secondary species, the governing partial differential equations can be written as

$$\frac{\partial(\phi C_j)}{\partial t} + \nabla \cdot (\mathbf{u}C_j - \mathbf{D}\nabla C_j) = R_j^{min} + R_j^{aq} \qquad (j = 1, \ldots, N_c) \tag{15}$$

$$\frac{\partial(\phi X_i)}{\partial t} + \nabla \cdot (\mathbf{u}X_i - \mathbf{D}\nabla X_i) = R_i^{min} + R_i^{aq} \qquad (i = 1, \ldots, N_x). \tag{16}$$

Eq (13), however, implies that the rate of production of a primary component j due to homogeneous reactions can be written in terms of the sum of the total rates of production of the secondary species (Kirkner and Reeves, 1988)

$$R_j^{aq} = -\sum_{i=1}^{N_x} \nu_{ij} R_i. \tag{17}$$

Eq (17) suggests that one can think of a mineral dissolving, for example, as producing *only primary species* which then equilibrate instantly with the secondary species in the system. Using eq (17), the rates of the reversible reactions can be eliminated if we make the simplifying assumption that the **D**'s are the same for all the aqueous species (Lichtner, 1985; Kirkner and Reeves, 1988). The use of differing diffusion coefficients for the various aqueous species requires special treatment in order to preserve electroneutrality (Lichtner, 1985). Multiplying eq (16) by ν_{ij} and summing over all the N_x secondary species yields

$$\frac{\partial}{\partial t}\left[\phi\left(\sum_{i=1}^{N_x} \nu_{ij}\mathrm{X}_i\right)\right] + \nabla \cdot \left[\mathbf{u}\left(\sum_{i=1}^{N_x} \nu_{ij}\mathrm{X}_i\right) - \mathbf{D}\nabla\left(\sum_{i=1}^{N_x} \nu_{ij}\mathrm{X}_i\right)\right] = -\mathrm{R}_j^{\mathrm{aq}}. \tag{18}$$

Adding eqs (15) and (18) gives a set of partial differential equations with N_c unknowns

$$\frac{\partial}{\partial t}\left[\phi\left(C_j + \sum_{i=1}^{N_x} \nu_{ij} X_i\right)\right] +$$

$$\nabla \cdot \left[\mathbf{u}\left(C_j + \sum_{i=1}^{N_x} \nu_{ij} X_i\right) - \mathbf{D}\nabla\left(C_j + \sum_{i=1}^{N_x} \nu_{ij} X_i\right)\right] = R_j^{min} \qquad (j = 1, \ldots, N_c) \tag{19}$$

In this particular example, only the term R_j^{min} remains on the right hand side of eq (19) because we have assumed that they are the only irreversible reactions. In the event that any of the homogeneous reactions are irreversible as well, they can be included on the right hand side in the same fashion (Lichtner, 1985).

If a total concentration, U_j, is defined (Reed, 1982; Lichtner, 1985; Kirkner and Reeves, 1988)

$$U_j = C_j + \sum_{i=1}^{N_x} \nu_{ij} X_i, \tag{20}$$

then the governing differential equations can be written in terms of the total concentrations (Kirkner and Reeves, 1988)

$$\frac{\partial(\phi U_j)}{\partial t} + \nabla \cdot (\mathbf{u} U_j - \mathbf{D} \nabla U_j) = R_j^{min} \qquad (j = 1, \ldots, N_c). \tag{21}$$

As pointed out by Reed (1982) and Lichtner (1985), the total concentrations can usually be interpreted in a straightforward fashion as the total elemental concentrations (for example, total aluminum in solution), but in the case of H^+ and redox species, the total concentration has no simple physical meaning and the total concentrations may take on negative values.

Redox reactions.—Using the formulation for a total dissolved concentration described above, redox reactions may be treated in the same fashion as any other complexation or precipitation/dissolution reaction (Reed, 1982; Lichtner, 1985). The only requirement is that the reactions involving oxidation/reduction processes be electrically balanced.

MINERAL PRECIPITATION/DISSOLUTION RATE LAWS

Transport versus surface-controlled reaction.—The kinetics of mineral precipitation and dissolution depend on (1) the rate of transport of various aqueous species to the surface of the mineral, and (2) the rate of attachment or detachment of ions from active sites on the mineral surface (Lasaga, 1990). A complete formulation of a quantitative precipitation/dissolution rate law, therefore, should include both transport and surface processes. Because such formulations are more complicated for multicomponent systems, however, it is customary to attempt to identify one of the processes, transport or surface attachment, as the *rate-limiting step* (Berner, 1980; Lasaga, 1981, 1986, 1990; Murphy, Oelkers, and Lichtner, 1988). Two limiting cases occur: where the transport to the mineral surface is much slower than the rate of attachment of ions at active sites, the mineral growth or dissolution is referred to as *transport-controlled,* whereas, in contrast, where the rate of attachment is much slower than the transport rate, the mineral growth and dissolution is termed *surface-controlled.* In many instances, both processes are of the same order of magnitude, and therefore neither can be properly referred to as the rate-limiting process.

The problem of determining whether surface attachment processes or transport processes dominate the growth and dissolution of a given crystal is more complicated in multi-component systems. In such systems, a number of separate components must be transported and attached or

detached from the crystal. The basic requirement that the rate of attachment or detachment must equal the rate of transport of the various components to the crystal is still present, but now we must also ensure that the diffusive flux of each component must be in the stoichiometric proportions corresponding to the overall reaction. This can be made clearer by using a simple example like that of albite precipitation. Assuming for simplicity that H^+, Na^+, Al^{+++}, and $SiO_{2,aq}$ are the only species present, the diffusive fluxes from the bulk solution into the albite crystal must be

$$J_{Na^+} = \frac{D_{Na^+}}{L}(C_{Na^+} - C_{Na^+,s}), \tag{22}$$

$$J_{H^+} = \frac{D_{H^+}}{L}(C_{H^+} - C_{H^+,s}), \tag{23}$$

$$J_{Al^{+++}} = \frac{D_{Al^{+++}}}{L}(C_{Al^{+++}} - C_{Al^{+++},s}), \tag{24}$$

$$J_{SiO_2} = \frac{D_{SiO_2}}{L}(C_{SiO_2} - C_{SiO_2,s}), \tag{25}$$

where L is the diffusion length scale, and where in each case the subscript s refers to the concentration of that species in solution *immediately adjacent* to the albite crystal whereas the unsubscripted concentration (for example, C_{SiO_2}) refers to the concentration of that ion in the bulk solution. In addition, the fluxes must be in their proper stoichiometric proportions with respect to albite, that is

$$J_{Na^+} = J_{Al^{+++}} = 3J_{SiO_2} = -4J_{H^+}. \tag{26}$$

As in the one-component system, a second requirement is that the fluxes match the attachment or detachment rate at the mineral surface which is given by

$$r_{alb}^{\circ} = A_{alb}\, k_{alb} f(C_s) = A_{alb} J_{Na^+}, \tag{27}$$

where A_{alb} is the surface area of albite, k_{alb} is the reaction rate constant for albite, and $f(C_s)$ is some (as yet unspecified) function of the concentrations next to the crystal surface. Because these concentrations adjacent to the crystal are *a priori* unknown, they must be determined *in addition to* the concentrations of the same species in the bulk fluid phase (that is, beyond the diffusion boundary layer next to the albite crystal). Since in eqs (26) and (27) we have 4 equations in 4 unknowns, we can always write eqs (22) through (25) in terms of a single diffusing species. Eq (26), therefore, allows us to eliminate all but one of the unknown species concentrations adjacent to the albite crystal. The resulting expression includes the combined effects of both diffusive transport and surface

attachment/detachment. In contrast to the single component case, however, a rate law applicable to a multi-component system means that in general we need to solve for the root of one additional polynomial for each reacting mineral in the system. While this is certainly feasible, the added complexity and computational expense which the combined rate law requires argued against using it in the present version of the reaction-transport code.

Surface control in multi-component systems.—In contrast to the difficulties posed by formulating a reaction rate law where transport plays a major role, surface-controlled growth or dissolution as a limiting case presents a much simpler problem from a computational point of view. This is because the ion concentrations that enter into the calculation of the ion activity product for surface-controlled dissolution or growth are just the concentrations of those ions in the bulk solution (for which we are solving). In this regard, a surface-controlled reaction rate law for mineral dissolution and precipitation requires the solution of the minimum number of equations equal to N_c, the number of independent components in the bulk fluid. In contrast, if a transport-controlled rate law is used, the minimum number of equations is $N_c + N_{min}$, where N_{min} is the number of minerals in the system.

In a general form, the rate of growth or dissolution of a mineral in aqueous solution can be expressed as

$$rate = Akf(a_i)f(\Delta G), \tag{28}$$

where A is the reactive surface area of the mineral of interest (for example, m^2 per m^3 total rock), k is the rate constant (moles formula units mineral per m^2 sec.), $f(a_i)$ is some function of the activities of the individual ions in solution, and $f(\Delta G)$ is some function of the free energy of the solution. The functions, $f(a_i)$, represent the inhibiting or catalyzing effect of various ions in solution which should be considered separately from the effect of the saturation state *per se*. This leads to the following form for the rate law of crystal growth and dissolution of a mineral (see Lasaga, 1981, 1984; Aagaard and Helgeson, 1982; Steefel and Van Cappellen, 1990)

$$r_m = sgn(\log [Q_m/K_m])A_m k_m(\prod_{i=1}^{N_c+N_x} a_i^p)\left|\left(\frac{Q_m}{K_m}\right)^{\mathscr{M}} - 1\right|^n, \tag{29}$$

where k is either the growth or dissolution rate constant, a_i is the activity of an inhibiting or catalyzing species raised to an empirically determined power p, and $\mathscr{M}$ and n are two positive numbers also normally determined by experiment. The bars | | refer to the absolute value of the quantity, and the term $sgn(\log Q_m/K_m)$ gives the sign of the expression: negative if the fluid is undersaturated and positive if the fluid is supersaturated with respect to the mineral. This formulation ensures that the reaction rate, r_m, has the correct sign when $n \neq 1$. This is in contrast to the expression given in Steefel and Van Cappellen (1990) (as pointed out by

Merino, Nahon, and Wang, 1993), although the correct expression was used in the calculations presented in that work. In this expression Q_m is the ion activity product written as

$$Q_m = \prod_{j=1}^{N_r} a_j^{\nu_{mj}}, \tag{30}$$

and K_m is the equilibrium constant for the mineral-water reaction written as the destruction of one mole of mineral m. The appropriate functional form for the dependence of the rate on the saturation state of the solution is the subject of a number of ongoing studies (Nagy and others, 1990; Van Cappellen and Berner, 1991; Nagy, Blum, and Lasaga, 1991; Nagy and Lasaga, 1992, Burch, Nagy, and Lasaga, 1993). Nonlinear rate laws for the mineral-water reactions (that is, m and/or $n \neq 1$) can have a profound effect on the behavior of a reactive flow system, particularly where they result in a significant decrease in the reaction rates close to equilibrium (Steefel and Van Cappellen, 1990; Kerrick, Lasaga, and Raeburn, 1991). Steefel and Van Cappellen (1990) used nonlinear rate laws for some of the minerals in their simulation of kinetically controlled weathering and found that they appeared to give more reasonable crystal growth rates than did the linear forms. A rigorous analysis of the effects of nonlinear rate laws on the behavior of reactive flow systems is a subject for future investigations. In the simulations presented in this paper, a linear form for all the reactions is used (that is, both m and $n = 1$).

The temperature dependence of the reaction rate constant can be expressed reasonably well via an Arrhenius equation (Lasaga, 1984). Since many rate constants are reported at 25°C, it may be more convenient to write the rate constant at some temperature as

$$k = k_{25}\, exp\left[\frac{-E_a}{R}\left(\frac{1}{T} - \frac{1}{298.15}\right)\right], \tag{31}$$

where E_a is the activation energy, k_{25} is the rate constant at 25°C, R is the gas constant, and T is temperature in the Kelvin scale.

Of the parameters that enter into the rate expression for a heterogeneous reaction, the reactive surface area or rock texture is in general the least constrained in natural systems. This is primarily because the surface areas of the reacting minerals are not constant with time (Steefel and Van Cappellen, 1990) or because the permeability structure of the medium has an effect on how much rock surface area is encountered by a particular volume of fluid. A rock permeability dominated by a few fractures of relatively wide aperture, for example, has only a small amount of surface area compared to the volume of fluid passing through it. The permeability structure of the rock may account for many of the apparent discrepancies between laboratory and field-determined mineral dissolution rates. It is clear that the amount of reactive surface area in real geological systems will turn out to be a complex function of the

properties of the particular rock of interest and, somewhat like hydrodynamic dispersion, will have to be determined through field studies on a case by case basis.

Any number of methods can be used to calculate reactive surface areas, although none of them has been verified in a natural system. One approach is to calculate the total surface area by computing or estimating the total number of mineral grains per unit area rock and an average grain radius (Lasaga, 1984). Steefel and Van Cappellen (1990) made use of a crystal size distribution to avoid averaging the grain radii. In addition, their method allowed for time-dependent generation of crystal nucleii, unlike the method of Lasaga (1984) which envisions nucleation as a single event. A disadvantage of both these approaches, taken by themselves, is that they don't explicitly account for the porosity structure of the rock. As pointed out by Phillips (1991), the porosity (and therefore by implication, the surface area) involves the size and distribution of pores rather than the distribution of grain sizes per se. The two are related only in the case of well-sorted, uncemented grains. The calculation of reactive surface areas, therefore, should be linked in some fashion to the porosity/permeability structure of the rock. The method used to calculate reactive surface areas in this study is discussed in the section on porosity-permeability relationships in fractured rock.

Calculating the changes in volume fraction for individual minerals is a more straightforward matter, since it does not depend on any particular mineral geometry or permeability structure. The change in the volume fraction of an individual mineral can be calculated directly from

$$\frac{d\phi_m}{dt} = V_m r_m, \tag{32}$$

where V_m is the molar volume of the mineral. From this expression, the porosity of the medium can immediately be obtained (if compaction and dilation are neglected), since

$$\phi = 1 - \sum_{m=1}^{N_m} \phi_m. \tag{33}$$

HEAT TRANSFER AND FLUID FLOW

Conservation of energy.—The conservation of energy can be written as a simple conduction-convection equation in which heat production and consumption due to chemical reactions or radioactive decay are neglected

$$\rho_m C_{p,m} \frac{\partial T}{\partial t} = \nabla \cdot (\lambda_m \nabla T - \rho C_{p,f} \mathbf{u} T), \tag{34}$$

where λ_m is the thermal conductivity of the bulk medium, T is the temperature, $\mathbf{u}$ is the Darcy flux, ρ_m and ρ are the densities of the bulk

medium and fluid respectively, and $C_{p,m}$ and $C_{p,f}$ are the specific heat capacities of the medium and fluid respectively.

Fluid continuity equation.—The fluid continuity equation is given by

$$\frac{\partial(\phi\rho)}{\partial t} = -\nabla \cdot (\rho \mathbf{u}), \tag{35}$$

if dehydration and hydration reactions are neglected. If the fluid is considered to be incompressible and if the porosity changes as a function of time are small (that is, the matrix is nearly incompressible), the expression for steady flow is reduced to

$$\nabla \cdot \mathbf{u} = 0. \tag{36}$$

The assumption of an incompressible fluid has been made here, with the density variations taken into account only in the gravitational body force term in eq (40) below (that is, we have assumed the Boussinesq approximation–Turcotte and Schubert, 1982).

Where the flow field is two dimensional and the flow is incompressible, it is convenient to make use of the stream function (Phillips, 1991). The fluid continuity equation in this case can be expressed in terms of the horizontal and vertical dimensions, x and z respectively, as

$$\frac{\partial u_x}{\partial x} + \frac{\partial u_z}{\partial z} = 0, \tag{37}$$

which is satisfied by the stream function defined as

$$u_x = -\frac{\partial \psi}{\partial z}, \qquad u_z = \frac{\partial \psi}{\partial x}. \tag{38}$$

The fluid continuity equation can be expressed in terms of the stream function and the temperature (Bear, 1972)

$$\frac{\partial}{\partial x}\left[\frac{1}{k_v}\frac{\partial \psi}{\partial x}\right] + \frac{\partial}{\partial z}\left[\frac{1}{k_h}\frac{\partial \psi}{\partial z}\right] = -\frac{g}{\mu}\frac{\partial \rho}{\partial x}, \tag{39}$$

where k_h and k_v are the horizontal and vertical permeabilities, and ρ is calculated from the equation of state described below. This formulation assumes that the principal directions of the permeability, k_h and k_v, are aligned with the coordinate directions x and z.

Darcy's law.—For geologic media, Darcy's Law is usually applicable, except in the case where flow occurs through fractures with a large aperture. Darcy's Law, which can be derived from the Navier-Stokes equation (Marsily, 1986), is given by

$$\mathbf{u} = -\frac{\mathbf{k}}{\mu}(\nabla P - \rho \mathbf{g}), \tag{40}$$

where **k** is the permeability tensor, μ is the dynamic viscosity, P is the fluid pressure, and **g** is the gravity vector [$\mathbf{g} = (0, 0, -g)$]. Darcy's law still applies where the fluid continuity equation is expressed in terms of the stream function (in which case the fluid pressure is eliminated from the conservation equation), but the fluid velocities are obtained directly from eq (38).

Equations of state.—The governing equations are complete when appropriate equations of state for density and viscosity are included. A full treatment would include density and viscosity as functions of temperature, pressure, and salinity, but only the effect of temperature is considered here. A fifth-order polynomial was fitted to the density data for pure water at 500 bars given in Helgeson and Kirkham (1974). For viscosity, a fifth-order polynomial was fitted to the data provided in Bruges, Latto, and Ray (1966), which applies to pressures corresponding to the water-saturation curve.

NUMERICAL METHODS

One of the principal reasons that few applications of multi-component reaction-transport have been considered is the daunting size of the system of equations that must be solved. For a multi-component chemical system solved numerically, every iteration requires the solution of a minimum of $N_c \times M$ equations, where N_c is the number of linearly independent chemical components in the system, and M is the number of grid points in the system. As noted above, this minimum applies when a surface-controlled reaction rate term is used. This suggests that in multi-dimensional systems, where the number of grid points needed to achieve some degree of accuracy is necessarily large, it will be important to use the most efficient numerical method in order to make the problem tractable.

One-step versus two-step schemes.—In terms of the numerical methods that could be used to solve multi-component reaction-transport problems, the most important distinction is between *one-step* methods, where the reaction and transport terms are solved simultaneously, and *two-step* methods, where the reaction and transport terms are either solved separately or in sequence (for a discussion, see Oran and Boris, 1987; Yeh and Tripathi, 1989, 1991; Mangold and Tsang, 1991). The accuracy of two-step approach (also referred to as operator splitting) depends on the degree of coupling between the reaction term and the transport terms within any one time step. If either the coupling is weak or the time step taken is very small, then the reaction terms and the transport terms may be solved separately. As pointed out by Yeh and Tripathi (1991), however, an accurate solution of the global set of equations normally requires iteration between the reaction and transport modules. In the two-step or "sequential iteration" approach employed by Yeh and Tripathi (1991), the iteration consists of sequentially solving the decoupled set of equations until convergence is obtained. In the one-step or global im-

plicit approach, the iterations involve a linearized set of global nonlinear equations.

The two-step approach has a number of potential or real advantages:

1. Separate routines for multi-component reaction and transport may be used. This has the advantage that it is possible to choose optimized routines which may introduce less numerical dispersion in advection-dominant problems, for instance. The decoupled methods, therefore, offer greater flexibility to the programmer.
2. There is no need to invert the very large matrices generated by the simultaneous solution of a coupled reaction and transport problem. Consequently, the memory requirements will be less than those for a fully coupled method.
3. The decoupled methods are generally easier to program, and it may be possible to take advantage of already available routines.
4. Because the set of matrix equations are smaller in the case of the two-step methods, they may be better conditioned (Yeh and Tripathi, 1991). This may be a significant advantage in the treatment of redox problems where the concentrations of the unknown concentrations may vary over many orders of magnitude.
5. These methods may be easier to develop for use on the new generation of parallel computers.

It is important to consider, however, some of the potential advantages of the one-step or *global implicit methods* (Kee and others, 1985). Of these, the most important are:

1. The *global convergence* properties of the fully coupled method may be better than the multi-step methods. Using a Newton method to solve the full set of equations, for instance, we expect to achieve quadratic convergence in the vicinity of a root, while we can expect linear convergence at best from the decoupled methods. Yeh and Tripathi (1991) point out that the sequential iteration method that they employ may require as many as 50 iterations within any one time step. The number of Newton iterations required for convergence is normally ≤ 10. .
2. It is sometimes possible to take larger timesteps with a fully implicit or coupled routine. This is particularly true where the governing differential equations are *stiff*, that is, when the time step needed to maintain numerical stability is much smaller than the time step needed for an accurate solution (Press and others, 1986). Stiffness arises in these kinds of differential equations primarily because of the different time scales represented by fast versus slow chemical reactions.

There are pros and cons to both methods, but the choice is less clearcut in favor of the decoupled methods than has been suggested by Yeh and Tripathi (1989), particularly where, as discussed above, widely differing rates of reaction result in a stiff set of equations. Their comparison of the

time required for the calculation of a single time step in the one-step and two-step approaches means very little without comparing the size of the time step and the convergence properties of the two methods as well. For an alternative viewpoint on the relative merits of the one-step versus two-step methods, see the review article by Kee and others (1985). We have chosen to pursue the fully coupled methods in this work.

A global implicit method for the reaction-transport equation.—Given the choice of an implicit or coupled method to solve the coupled reaction-transport equation, there are still a number of possible approaches that can be used. Following the notation of Lichtner (1992), we can introduce the differential operator

$$\mathscr{L}(U_j) = \left[\frac{\partial}{\partial t}\phi + \nabla(\mathbf{u} - \mathbf{D}\nabla)\right]U_j \tag{41}$$

and write the governing differential equations in terms of the total component concentrations as

$$\mathscr{L}(U_j) = R_j^{min} \qquad (j = 1, \ldots, N_c), \tag{42}$$

where the reaction term R_j^{min} includes only irreversible (in our case, heterogeneous) reactions. Note that in this formulation, we assume that the diffusion coefficients are the same for all the aqueous species (both primary and secondary). This makes the solution of the reaction-transport equation much simpler, because the secondary species do not have to be transported individually.

As discussed by Kirkner and Reeves (1988), one way to proceed at this point would be to solve directly for the total component concentrations (the U_j's), thereby decoupling the solution of the differential equations from the speciation calculations. In this formulation (formulations B and C of Kirkner and Reeves, 1988), every iteration to solve for U_j is preceded by an equilibrium speciation calculation to determine the concentrations of both primary and secondary species. On the basis of a number of preliminary benchmark tests (not reported here), however, it appears that the most robust solution method directly couples the speciation calculations to the differential equations to obtain an expression for the total component concentration in terms of the primary species alone. A similar conclusion was reached by Reeves and Kirkner (1988) who carried out a much more extensive set of benchmarks. Substituting this result into eq (42) gives (essentially a kinetic version of formulation A of Kirkner and Reeves (1988))

$$\mathscr{L}\left[C_j + \sum_{i=1}^{N_x} \nu_{ij}\gamma_i^{-1}K_i^{-1}\prod_{j=1}^{N_c}(\gamma_j C_j)^{\nu_{ij}}\right] + \sum_{m=1}^{N_m} \nu_{jm}\,\mathrm{sgn}\,(\log[Q/K_m])A_m k_m\left|\left(\prod_{j=1}^{N_c}(\gamma_j C_j)^{\nu_{mj}}K_m^{-1}\right)^{\sigma} - 1\right|^n = 0, \tag{43}$$

where the γ_i's and γ_j's are the activity coefficients for the secondary and primary species respectively and where we have neglected the inhibiting or catalyzing effects of the various aqueous species for the sake of compactness. If eq (43) is discretized on a grid using M nodal points (see below), for instance, then the total number of equations to be solved is $N_c \times M$, where N_c is the number of primary species in the system. Note that this method is a variant of the differential and algebraic equation (DAE) approach using the concentrations of component and precipitated species as the primary dependent variables (PDVs) discussed by Yeh and Tripathi (1989; 1991). Because of the form of the mineral-fluid reaction rate law as expressed in eq (29), however, the concentration of precipitated species can be expressed directly in terms of the concentrations of primary species.

Finite difference discretization.—The set of partial differential equations represented by eq (43) can be discretized using any number of schemes (see, for example, Patankar, 1980; Lapidus and Pinder, 1982; Press and others, 1986; Marsily, 1986). The integrated finite difference or control-volume method is a particularly flexible one which easily includes variable grid spacing and non-constant diffusion coefficients or fluid velocities (Narasimhan and Witherspoon, 1976; Patankar, 1980; Marsily, 1986). In the integrated finite difference formulation, a control volume is defined within which the partial differential equation must be satisfied in the average. A Taylor series expansion in terms of neighboring nodes is used to represent the spatial derivatives that appear in the flux terms (fig. 1), thus converting the differential equations to a set of algebraic equations. The reaction terms, which by themselves make up a set of ordinary differential equations that are functions of time, represent an average over the control volume. In one dimension, therefore, the unknown or unknowns (in this case, the N_c primary species concentrations) at grid point P are coupled via linear transport coefficients to the two neighboring grid points, W and E (that is, upstream and downstream

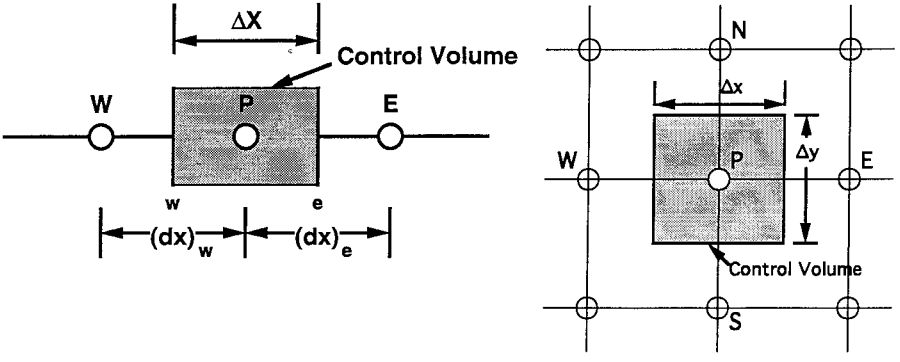

Fig. 1. Control volumes for one and two-dimensional systems.

in the case of flow). In a two dimensional system, each grid point within a control volume is linked to 4 adjacent grid points where the flow is parallel to one of the coordinate axes and to 8 neighbors where flow not parallel to a coordinate axis results in an anisotropic dispersion tensor (Marsily, 1986).

Typically the greatest difficulty in using Eulerian or fixed grid methods to represent solute transport occurs where advective transport is dominant. This is because the use of the central difference method of representing the first derivative that appears in the advection term (Lapidus and Pinder, 1982) may result in non-physical oscillations in the vicinity of sharp concentration fronts (Patankar, 1980; Daus and Frind, 1985; Frind and Germain, 1986; Patel, Cross, and Markatos, 1988). The performance of a particular finite difference formulation for the first derivative depends in part on the relative magnitudes of the advection and dispersion/diffusion terms. The relative importance of the two can be described by the dimensionless *grid Peclet number* given by (Daus and Frind, 1985; Patel, Cross, and Markatos, 1988)

$$Pe_{grid} = \frac{\upsilon \Delta x}{D} \tag{44}$$

where Δx refers to the grid spacing at any particular point in space. Only for $Pe_{grid} < 2$ is the central difference formulation unconditionally stable (Daus and Frind, 1985; Frind and Germain, 1986; Patel, Cross, and Markatos, 1988). The problem of stability can be "cured" by using a forward difference formulation written in terms of the grid point itself and the *upstream* or *upwind* node (Press and others, 1986). The upstream-weighted formulation, however, achieves its greater stability essentially by adding numerical dispersion (that is, over and above the physical dispersion present in the problem), in addition to having a larger truncation error than the central difference method. The problem is most severe in multi-dimensional problems where flow is diagonal to rather than along the direction in which the nodes are distributed (Patel, Cross, and Markatos, 1988) and in problems where transient, sharp concentration fronts occur. Higher order schemes are necessary to eliminate or reduce these effects.

In this work, a "power law scheme" proposed by Patankar (1980) is used to represent the transport terms in the finite difference approximation. The method slides between a fully centered form at $Pe_{grid} < 2$ to an upstream-weighted formulation at $Pe_{grid} > 10$, where the upwind scheme is necessary for stability (Patankar, 1980). Because the scheme does not eliminate numerical dispersion, however, the code as presently written is not ideal for treating problems where very accurate representations of transient concentration fronts are necessary.

Since it is difficult to choose the coordinate axes of the finite difference grid so that one of the axes is everywhere parallel to the flow direction, the dispersion tensor will locally contain off-diagonal terms. In

this case, for Cartesian coordinates, an average velocity $|U|$, and the velocity components $|U|_x$ and $|U|_z$, the elements of the dispersion tensor are (Bear, 1979)

$$D_{xx} = \alpha_T|U| + \frac{(\alpha_L - \alpha_T)|U|_x^2}{|U|} \tag{45}$$

$$D_{zz} = \alpha_T|U| + \frac{(\alpha_L - \alpha_T)|U|_z^2}{|U|} \tag{46}$$

$$D_{xz} = \frac{(\alpha_L - \alpha_T)|U|_x|U|_z}{|U|}. \tag{47}$$

As discussed above, the off-diagonal coefficients are multiplied by cross-derivative terms requiring the use of a 9 point finite difference operator.

Solution method.—Since both the total component concentrations, U_j, and the heterogeneous reaction term, R, are nonlinear functions of the primary species concentrations, an iterative method is required to solve it. The nonlinear set of algebraic equations are solved with the Newton-Raphson method, which makes use of a Taylor series expansion to linearize the set of nonlinear equations. In practice, one carries out a series of nested calculations in order to complete a single time step. A number of Newton iterations are normally required to obtain convergence of the nonlinear set of algebraic equations. Each Newton iteration, in turn, requires the solution of a set of simultaneous linear equations at each nodal point within the domain in order to obtain the corrections to the primary species concentrations (app. 1). If we consider a one-dimensional system for the sake of simplicity, it is apparent that the concentrations of the primary species at a nodal point P are potentially functions of all the primary species concentrations at the P, E, and W nodal points (fig. 1). Therefore, each function, f_j, representing a conservation equation for a total component concentration U_j at a nodal point P, must be expanded in terms of the primary species concentrations at the three neighboring grid points. The logarithms of the primary species concentrations are used because of the superior numerical stability of this method. In a one-dimensional problem, a single Newton iteration requires solving a set of linear equations of the form

$$\sum_{j'=1}^{N_c} \frac{\partial f_{j,P}}{\partial \ln C_{j',P}} \delta \ln C_{j',P} + \sum_{j'=1}^{N_c} \frac{\partial f_{j,P}}{\partial \ln C_{j',E}} \delta \ln C_{j',E} + \sum_{j'=1}^{N_c} \frac{\partial f_{j,P}}{\partial \ln C_{j',W}} \delta \ln C_{j',W} = -f_{j,P}, \tag{48}$$

where the derivatives $\partial f_j/\partial \ln C_{j'}$, form the elements of the *Jacobian* matrix. Once the entire vector of concentration corrections (the $\delta \ln C_{j'}$'s)

are obtained by solving eq (48) over the entire spatial domain, the concentrations are updated according to

$$\ln C_{j'}^{k+1} = \ln C_{j'}^{k} + \delta \ln C_{j'}, \tag{49}$$

where the superscript k refers here to the iteration level. This procedure is repeated until convergence is obtained. A block SOR method is used to solve the set of linear equations within each Newton iteration and is discussed more fully in app. 1.

The mineral volume fractions and surface areas are held constant over a single time step and are updated only once convergence of the concentrations of the primary species has occurred. This procedure is justified computationally in the vast majority of cases because the mineral volume fractions change much more slowly than do the solute concentrations in the fluid. The mineral volume fractions are obtained by writing eq (32) in finite difference form

$$\phi_m^{n+1} = \phi_m^n + r_m^{n+1} V_m \Delta t, \tag{50}$$

where n and $n + 1$ refer to the previous and present time levels respectively, and Δt is the time step. The update of the mineral surface areas depends on the particular formulation adopted. A method for calculating surface areas in a fractured rock is discussed in the section on *Applications* below.

PROGRAM STRUCTURE

The structure of the code used to solve the set of conservation equations for solute mass is summarized in figure 2. To begin the calculation, the geometry of the region and its material properties must be defined. Initial and boundary conditions for the aqueous species, mineral volume percentages, temperature, and flow are then specified. At this point, the code begins stepping through time. Where the flow and/or temperature field are not given in advance, they are calculated first. If there is little or no feedback between the solute concentration equation and the hydrodynamic flow, then the solute concentrations can be solved after the flow and temperature. Where strong coupling is present, as for example in the case where chemical reactions have a significant effect on the solution density, then iteration between the flow and the solute concentration is required. Alternatively, one could continue to use the "operator splitting" technique and simply reduce the size of the time step so that relatively little density change due to solute reaction and transport occurs in any one time step. The splitting approach as presently used also assumes that very little porosity and permeability change occurs in any one time step.

Following the calculation of the flow and temperature fields, the solute transport coefficients are computed using the formulation given by Patankar (1980) described above. A check is made at this time to see whether basis switching is needed at any node within the system. If so, the reactions are rewritten locally in terms of the dominant species and redox

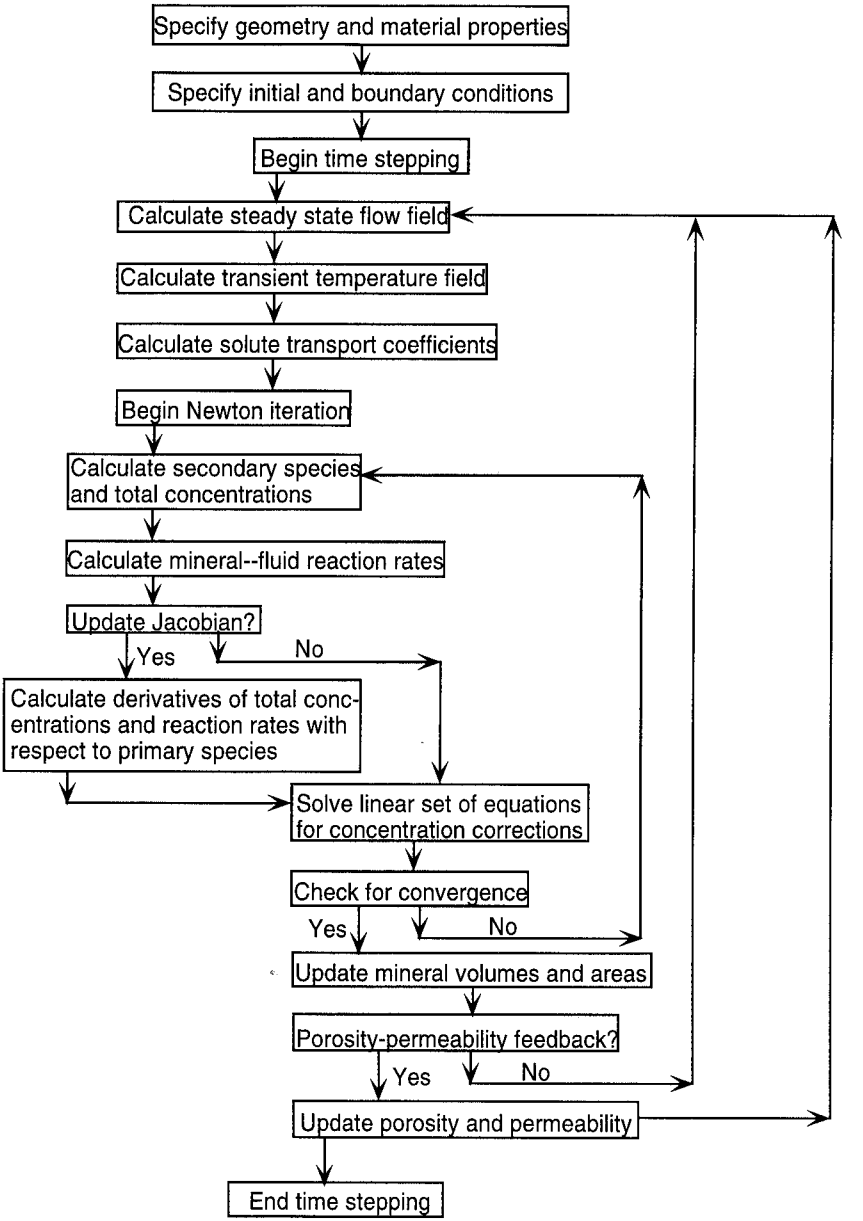

Fig. 2. Program structure used to calculate coupled multi-species chemical, heat, and fluid transport and multi-component geochemical reactions.

couple. At this point, a series of Newton iterations is required in order to solve for the solute concentrations at the new time level (fig. 2). Each Newton iteration consists of calculating the function residuals (the $f(x_i)$'s given by eq 43) and the partial derivatives of these functions (the Jacobian elements) with respect to the unknown concentrations and then assembling and solving the linear set of $N_c \times M$ algebraic equations (app. 1) in order to obtain the corrections to the component concentrations (eqs 48 and 49). As discussed above, the functions include both the contributions from homogeneous and heterogeneous reactions and from advective, dispersive, and diffusive transport which are evaluated at each grid point within the system. This is repeated until convergence is achieved, that is, to the point where the $f(x_i)$'s are all reduced to some desired tolerance. It is usually not necessary to update the matrix of partial derivatives every iteration, since the Jacobian matrix does not have to be exact. Instead, the Jacobian is typically recalculated when the number of Newton iterations required to achieve convergence exceeds some specified tolerance (Kirkner and Reeves, 1988). This method (referred to as a modified Newton method) can be particularly efficient since it is the assembly of the Jacobian elements that takes a large part of the CPU time (Kee and others, 1985). Once convergence of the Newton iterations is achieved, the mineral volume fractions and mineral surface areas are updated. If one chooses to make use of the quasi-stationary state approximation (Lichtner, 1988), then the mineral volume fractions and surface areas are updated *only* when a quasi-stationary state with respect to the fluid concentrations has been achieved, rather than after every time step. If the porosity and permeability of the medium are allowed to change with time, they are updated at this time if the code is run in transient mode. At the end of each time step, whether the code is run in either the quasi-stationary or transient mode, an algorithm, which computes the second derivative of the solute concentrations with respect to time, is used to determine whether the time step should be increased or decreased. This algorithm provides a way of minimizing the time truncation error (if that is an issue in a particular problem) and also of controlling the size of the time step so as to maintain numerical stability. As the solute concentration profile relaxes to a steady state, the time step gradually increases to some specified maximum value (5 yrs in the simulations presented in this paper).

APPLICATION TO REACTIVE FLOW IN HYDROTHERMAL SYSTEMS

In this section, we use the one and two-dimensional numerical model described above to examine two important problems related to reactive flow in hydrothermal systems. First, we use reactive transport calculations to assess the validity of the local equilibrium assumption in nonisothermal flow systems. Although it is not possible to describe all the possible reactive flow systems likely to be found in nature, by considering a range of conditions as might exist in continental or submarine hydrothermal systems, it is possible to place some broad constraints on where

the local equilibrium assumption is likely to be justified and where it is likely to break down. Secondly, we use two-dimensional calculations to investigate the rate of permeability change due to geochemical reactions in a fracture-controlled hydrothermal system. Of particular interest is how the time scales for reaction-induced permeability change compare with the time scales for evolution of the hydrodynamic and thermal regimes.

Most of the theoretical studies to date on hydrothermal systems developed in the shallow portions of the Earth's crust have focused on the physics of hydrodynamic flow. Relatively little research, however, has been devoted to quantitative studies of coupled reaction and solute transport in hydrothermal systems. Only a few studies of either fossil or active hydrothermal systems have explicitly considered the role of transport processes in determining the geochemical character of a particular hydrothermal system. Norton and Taylor (1979) carried out simulations of the Skaergaard intrusion in Greenland in which the hydrodynamic flow and heat transfer were coupled to isotopic exchange. Cathles (1983) performed similar calculations in studying the formation of Kuroka-type massive sulfide deposits. Wood and Hewett (1982) analyzed qualitatively the spatial distribution of precipitation and dissolution zones resulting from convection in a sloping limestone layer. Wells and Ghiorso (1991) investigated the problem of quartz dissolution and cementation in mid-ocean ridge systems. Phillips (1991) presented a general study of the fundamentals of flow and reactions in hydrothermal systems and applied his methodology to the dolomitized reef complex at Lattemore, Italy (Wilson, Hardie, and Phillips, 1990). Steefel and Lasaga (1992) presented what may be the first two-dimensional simulations of multi-component and multi-mineralic reactive flow in a hydrothermal system, focusing on the chemical effects of fluid mixing resulting from hydrodynamic dispersion.

Flow in hydrothermal systems is either partly or wholly driven by horizontal temperature gradients, although imposed hydraulic head gradients may modify the flow (Elder, 1965; Norton and Knight, 1977; Norton and Cathles, 1979; Phillips, 1991; Lowell, Van Cappellen, and Germanovich, 1993). Any horizontal density gradient can drive convection, including those due to salinity variations, but high temperature convection cells generated in the shallow portions of the crust can generally be attributed to the presence of magma bodies at depth. Examples are the geothermal fields developed in continental settings (for example, Broadlands, New Zealand and Yellowstone Park, United States of America; White, Muffler, and Truesdell, 1971; Truesdell and Fournier, 1976; Elder, 1981; Fournier, 1989; Lowell, 1991) and the submarine systems that form at mid-ocean ridges or ridge flanks (Anderson, Langseth, and Sclater, 1977; Fehn and Cathles, 1986; Davis and others, 1989; Lowell, 1991). The imposed temperature gradients not only drive convection, they also exert an important influence on the character of reactive hydrothermal systems through the temperature dependence of mineral

solubilities, aqueous species stabilities, and chemical reaction rates. The reactions that occur in nonisothermal systems can be classified as *gradient* reactions (Wood and Hewett, 1982; Phillips, 1991; Ferry and Dipple, 1991), since they occur either partly or wholly because of gradients in temperature and/or pressure. As discussed by Phillips (1991), gradient reactions can occur simultaneously throughout the rock wherever the flow crosses temperature and/or pressure gradients and are therefore unlike isothermal reactions that propagate through the rock as coherent fronts (Lichtner, 1988; Steefel and Van Cappellen, 1990).

The local equilibrium approximation has long been a fundamental tenet of most geochemical and petrologic studies of hydrothermal systems. It has not been adequately demonstrated to date, however, that the reaction rates of the important rock-forming minerals are sufficiently rapid that the local equilibrium assumption is justified, particularly given the rapid flow rates that may occur. What are the important parameters that determine whether the local equilibrium approximation is justified in a particular hydrothermal system? Knapp (1989) carried out an interesting review of this problem in a wide variety of geological environments using the nondimensional Damkohler number, given by

$$Da = \frac{k'l}{u}, \tag{51}$$

where k' (T^{-1}) is the effective rate constant (including the surface area effect), and l is the length scale of interest. To obtain a more realistic assessment of how valid the equilibrium assumption is in specific geologic environments, however, it is necessary to consider both the local flow rates and temperature gradients. As demonstrated below, the presence of temperature gradients may impose local length scales that have nothing to do with the size of the system as a whole.

A second important issue is how the chemical reactions driven by the transport of solutes across temperature gradients affects the porosity and permeability of the hydrothermal convection cell. A number of the early theoretical studies of convection in the crust examined the transient evolution of the convection cells without considering whether the permeability will remain constant within the time scale of interest. Since reaction-induced permeability changes may alter the entire character of the hydrodynamic flow and temperature regimes, it is important to have a first-order idea of how rapidly the porosity and permeability are likely to change given a particular hydrothermal system. At this stage it is impossible to carry out a truly realistic simulation of the porosity and permeability change in natural geologic environments. This is primarily because there is little information at this point on how precipitation and dissolution reactions will affect permeability. Precipitation of quartz, for instance, may occur locally along pore throats, thus producing a large reduction in the permeability for a relatively small change in the porosity of the rock. To carry out a calculation of reaction-induced permeability change at this stage, one must assume a highly idealized fracture geom-

etry. We assert, however, that these idealized calculations are still valuable in analyzing some of the first-order effects associated with reaction-induced permeability change, just as the simulations of convection in hydrothermal cells, which ignored the problem completely, were instructive in elucidating some of the fundamental physics associated with convection in the crust.

Thermally-driven reactive flow.—Before proceeding to the analyses of the problems discussed above, it is useful to consider which parameters, physical and chemical, are important in determining the behavior of nonisothermal reactive flow. An excellent review of the fundamental parameters determining the physics of thermally driven flow and equilibrium reactions is given by Phillips (1991). One can describe much of the physical behavior of a particular hydrothermal system with the use of the nondimensional Rayleigh number along with the scale ratio, $S = (h/l)^2(k_h/k_v)$ (Phillips, 1991), where h refers to the depth of the system, l is its horizontal extent, k_h is the horizontal permeability, and k_v is the vertical permeability. The Rayleigh number is given by (Turcotte and Schubert, 1982; Phillips, 1991)

$$Ra = \frac{\alpha g \rho_0^2 C_{p_f} k h \Delta T}{\mu \lambda_m}, \tag{52}$$

where α is the thermal expansivity, ρ_0 is the reference density of water, h is the vertical extent of the system, ΔT is the temperature between the upper and lower boundary, and all the other parameters are the same as defined in eqs (34) and (40). The use of the nondimensional Rayleigh number and scale factor as the important parameters to describe the physics of convection implies that we need not concern ourselves with the specific values of the permeability in a particular system (Phillips, 1991). As we shall see below, however, while the Rayleigh number and scale factor determine the character of the hydrodynamic and temperature regimes, additional information is needed to specify the behavior of a reactive solute. The solubility of most minerals depends strongly on the absolute magnitude of the temperature and under some conditions, the fluid pressure. This implies, therefore, that the behavior of a high temperature system will be different from a lower temperature system with an identical Rayleigh number. Obviously, the temperature dependence of the reaction rates can have a similarly profound effect. Another important factor, which does not appear in either the Rayleigh number or the scale factor, is the amount of reactive mineral surface area in the system. In a fracture-dominated system, this depends at least in part on the spacing of fractures in the rock. These effects are discussed more fully in the following section which describes the model used for porosity and permeability in a fractured rock.

Porosity-permeability model for fractured rock.—In order to couple the porosity changes due to chemical reactions calculated from eqs (32) and (33), we need a model that relates the porosity of the medium to its permeability. In addition, the amount of mineral surface area encoun-

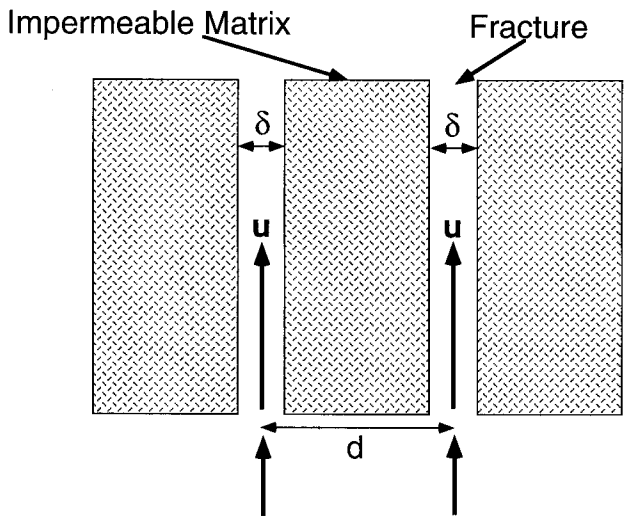

Fig. 3. Schematic drawing showing a single set of parallel fractures with constant apertures, δ, and constant spacing, d. The model assumes that the rock matrix is effectively impermeable, that is, that reactions and transport occur only within the fractures. The total surface area corresponds to the surface area of the fracture walls.

tered by a volume of fluid may be affected by the porosity-permeability relationship appropriate for a particular rock. A fluid moving through a large fracture, for example, will encounter far less mineral surface area per unit volume fluid than will a fluid moving through a relatively homogeneous rock like a porous sandstone. The simplest possible porosity-permeability model for fractured media is that of a set or sets of parallel fractures with smooth walls (Snow, 1970; Norton and Knapp, 1977; Marsily, 1986; Pruess, Wang, and Tsang, 1990; Phillips, 1991). In this model, the fracture (also referred to as the kinematic or flow) porosity contributed by a single set of parallel fractures is given by

$$\phi_F = \frac{\delta}{d}, \tag{53}$$

where δ is the fracture aperture, and d is the fracture spacing (= $1/n$, where n is the fracture density) (fig. 3). This formulation also provides an expression for the rock permeability for a single set of fractures (Norton and Knapp, 1977; Phillips, 1991)

$$k = \frac{\delta^3}{12d}, \tag{54}$$

or written in terms of the fracture porosity,

$$k = \frac{\phi_F \delta^2}{12}. \tag{55}$$

If more than a single set of parallel fractures is present, then the fracture porosity is given by

$$\phi_F = \sum_{i=1}^{NF} \frac{\delta_i}{d_i}, \tag{56}$$

where N_F is the number of fracture sets, and the subscript i refers to the individual fracture sets. This simple formulation, however, slightly overestimates the porosity since it doesn't account for the intersection of the various fracture sets (that is, the voids where the fractures intersect are counted twice). For the case in which three sets of mutually orthogonal fractures are present, thus producing an isotropic permeability, and where all the fracture sets have the same spacing and fracture apertures, $\phi_F = 3\delta/d$. The scalar permeability in this case is (Phillips, 1991)

$$k = \frac{\phi_F \delta^2}{36}. \tag{57}$$

This formulation is used in the two-dimensional simulations described below. Expressions for porosity-permeability models for fractured rocks that do not assume an isotropic permeability may be found in Marsily (1986).

We can also use the porosity-permeability model described above to calculate mineral surface areas if several additional assumptions are made. The most important of these assumptions is that the reactions taking place in the rock occur exclusively along the fracture walls and *not* within the rock matrix bordering the fractures. While this will in general only be true where the rock bordering the fractures has a very low porosity, thus resulting in low diffusivities of the reacting solutes in the rock matrix, a simultaneous treatment of flow in fractures and matrix diffusion is beyond the scope of the present study. The assumption that the reactions are restricted to the fracture walls has two important consequences. First, the sum of the mineral surface areas must equal the total surface area of rock in contact with the fluid. For fractures with smooth walls and the same aperture, the ratio of the rock surface area to the fluid volume in a fracture, A_F, is

$$A_F = \frac{2}{\delta}. \tag{58}$$

The total surface area in contact with fluid per unit volume rock (rather than per volume fluid), A_{tot}, is therefore

$$A_{tot} = \phi_F \frac{2}{\delta}. \tag{59}$$

In the case of a single set of parallel fractures, then

$$A_{tot} = \frac{2}{d}. \tag{60}$$

This indicates that the total surface area of rock in contact with fluid in one or more identical fracture sets depends on the fracture spacing, d.

It is less clear, however, how to calculate the surface areas of individual minerals using the formalism described above. One can imagine a number of scenarios where one mineral accounts for most of the surface area along a set of fractures, even though other minerals are present in the rock. This might be the case, for example, where quartz precipitation occurs on the fracture wall. Because the surface area of minerals lining the fracture walls need not bear much relationship to the bulk mineralogy of the rock, it is more useful to obtain the fraction of the surface area occupied by any one mineral by considering the average grain size of the minerals that may evolve with time. If a mineral is either absent from the rock or undersaturated with respect to the solution, then its average radius is considered to be zero. We assume for the sake of simplicity that if a mineral is initially absent from the rock but becomes supersaturated, it instantaneously acquires a radius of 10 microns which then evolves with time according to

$$\frac{\partial rad_m}{\partial t} = \frac{1}{A_m}\frac{\partial \phi_m}{\partial t}, \tag{61}$$

where rad is the mineral radius, and $\partial rad_m/\partial t$ is the average linear growth rate for the mineral m. The surface area of the mineral, A_m, is then obtained for any one time step from

$$A_m = \frac{rad_m^2}{\sum_{m=1,N_m} rad_m^2} A_{tot}, \tag{62}$$

where N_m is the number of minerals in the system. Note that this formulation ensures that the reactive surface area of a mineral accessible to fluid cannot exceed the total surface area along the fracture walls.

Using this porosity-permeability relationship, we can calculate the reaction-induced changes in rock permeability as a function of time. The assumption that the mineral-water reactions take place exclusively along the fracture walls means that the change in the mineral volumes with time affects the walls of the fractures only. In other words, since the rock matrix is assumed to be nearly impermeable, precipitation and dissolution cannot occur in isolated pores within the matrix. A second assumption made is that there is no distribution of fracture apertures (that is, within any one elemental volume they are assumed to be all of the same size). As the porosity and permeability evolves in the simulations, however, variations in fracture aperture develop in space. Additionally, we assume that the fractures retain smooth, parallel walls throughout the course of the simulation. We also assume that the permeability remains isotropic through the course of the two-dimensional simulations.

Porosity-permeability ranges in fractured rocks.—There have been a number of attempts to estimate porosity-permeability relationships in,

fractured rocks. Norton and Knapp (1977), using a planar fracture model of the kind described above, estimated that fracture porosities had a total range between 1 and 5×10^{-6} percent, although the more common range they observed was between 0.1 and 0.001 percent. These estimates are derived from their measurements of the fracture density (or fracture spacing) and fracture apertures which are summarized in table 1. Pruess, Wang, and Tsang (1990), citing studies by Scott and others (1982) and Peters and others (1984), report that the fracture spacing at the Yucca Mountain site in Nevada is on the order of 0.3 m and fracture apertures range from about 10 to 100 μm. Manning and Bird (1991) measured cumulative vein densities (d^{-1} or n) in the contact aureole of the Skaergaard intrusion in Greenland and found that the fracture apertures ranged from about 100 to 1000 μm with the more common value being closer to 100 μm. A value of 100 μm was assumed by Manning and Bird (1991) in their calculations. Table 1 gives the fracture spacings and the contributions to the total fracture porosity given by the individual fracture sets recorded by Manning and Bird (1991). Note that Manning and Bird (1991) actually give the porosities as simple fractions and not as percents.

TABLE 1

Estimates of fracture spacing, fracture aperture, and fracture porosities in natural environments

Fracture Porosity (%)	Fracture Aperture (μm)	Fracture Spacing (m)	Reference
5×10^{-6} to 1	0.5 to 200	10 to 0.22	1
0.029*	64	0.22	2
0.285*	100	0.035	3
0.016*	100	0.625	4
0.182*	100	0.055	5
0.021*	7.5	0.035	6
0.003*	19	0.625	7
0.016*	8.7	0.055	8

1. Norton and Knapp (1977)
2. Pruess, Wang, and Tsang (1990)
3. Average of 6 horizontal veins, Skaergaard Intrusion (Manning and Bird, 1991) assuming a fracture aperture of 100 μm.
4. Average of 16 vertical pyroxene veins, Skaergaard Intrusion (Manning and Bird, 1991) assuming a fracture aperture of 100 μm.
5. Average of 22 vertical amphibole veins, Skaergaard Intrusion (Manning and Bird, 1991) assuming a fracture aperture of 100 μm.
6. Average of 6 horizontal veins, Skaergaard Intrusion (Manning and Bird, 1991) using permeability of 10^{-15} m^2 determined by Norton and Taylor (1979) (fracture aperture calculated from eq 54).
7. Average of 16 vertical pyroxene veins, Skaergaard Intrusion (Manning and Bird, 1991) using permeability of 10^{-15} m^2 determined by Norton and Taylor (1979) (fracture aperture calculated from eq 54).
8. Average of 22 vertical amphibole veins, Skaergaard Intrusion (Manning and Bird, 1991) using permeability of 10^{-15} m^2 determined by Norton and Taylor (1979) (fracture aperture calculated from eq 54).

* Porosities represent contribution from a single fracture set.

As pointed out by Norton and Knapp (1977), the determination of the fracture apertures is uncertain at best, since the present width of the fracture, which represents the cumulative width of precipitates and/or open space, need not actually have been the fracture aperture during hydrothermal activity. In addition, one expects that there is a pressure effect at depth that would tend to reduce the fracture aperture. In the case of the Skaergaard intrusion, there is another way to estimate what the fracture apertures are likely to have been during the hydrothermal event. Norton and Taylor (1979), based on hydrodynamic flow and thermal modeling of the Skaergard intrusion combined with a model for isotopic exchange, were able to estimate an average permeability of about 10^{-15} m^2 for the rocks surrounding the intrusion by comparing model results with the observed isotopic patterns. If we assume that their permeability determination is approximately correct and if we also assume a porosity-permeability model based on an isotropic assembly of fractures all of the same aperture and spacing, then we can calculate fracture apertures from eq (54) using the fracture spacings reported by Manning and Bird (1991). These calculations are also given in table 1. As an example, if we use the fracture spacing for the 22 vertical amphibole veins reported by Manning and Bird (1991) for the Skaergaard and assume that this particular fracture set is duplicated in the second and third dimension, then one calculates a fracture aperture of 8.7 μm and a total fracture porosity of 0.048 percent. Note that this fracture aperture is about an order of magnitude less than the present width of mineral precipitate and open space observed by Manning and Bird (1991).

Validity of the local equilibrium approximation in thermal boundary layers.—As discussed above, the extent to which the local equilibrium approximation may be valid for a particular system depends in part on

TABLE 2

Physical parameters used in hydrothermal simulations

Top boundary temperature	50°C
Lower boundary temperature (at center)	300°C
Depth of system (h)	2980 m
Half-width of system (l)	5840 m
Longitudinal dispersivity (α_L)	10 m
Transverse dispersivity (α_T)	1 m
Thermal conductivity (λ_m)	3 W m^{-1} °K^{-1}
Heat capacity of fluid ($C_{p,f}$)	4200 J kg^{-1} °K^{-1}
Heat capacity of rock ($C_{p,m}$)	1005 J kg^{-1} °K^{-1}
Average rock density (ρ_m)	2600 m^3 kg^{-1}
Thermal diffusivity (κ)	1.15×10^{-6} m^2 s^{-1}
Reference fluid density (ρ_{50})	1000 m^3 kg^{-1}
Gravitational constant (g)	9.8 m s^{-2}
Thermal expansivity (α)	10^{-3} °K^{-1}
Average dynamic viscosity (μ)†	2×10^{-4} Pa s

† Value used in Rayleigh number calculations and in eq (64). A temperature-dependent viscosity is used in the numerical simulations.

the Damkohler number (eq 51), which compares the characteristic time for reaction with the characteristic time required for a solute particle to traverse a certain length scale. When considering nonisothermal systems, however, it is important to recognize that the flow rate can influence the local temperature gradients as well. Since the equilibrium solubility of most rock-forming minerals depends strongly on temperature, sharp temperature gradients can result in sharp gradients in the equilibrium constants as well. In other words, unlike the isothermal case where one can view the solubility as a fixed quantity independent of space, in the nonisothermal case the solubility of a mineral *may* be a function of space locally. The sharper the local temperature gradient, the greater the possibility that equilibrium will be overstepped as a fluid packet traverses that distance. For this reason, the analysis of Wells and Ghiorso (1991) does not really yield any insight into the validity of the local equilibrium approximation, since the flow rate in their study is not allowed to influence the temperature field.

It is possible to obtain some order of magnitude estimates of the degree of disequilibrium one is likely to encounter in a hydrothermal upflow zone by considering an idealized case in which the buoyant flow is locally one-dimensional. An example discussed by Lowell, Van Cappellen, and Germanovich (1993) is that of the Sea Cliff hydrothermal field on the northern Gorda Ridge in the Pacific Ocean. Here discharging hydrothermal waters result in a thin crust of precipitated silica at the ocean floor where the heated fluids encounter cold seawater. Lowell, Van Cappellen, and Germanovich (1993) studied the rate of fracture closing with the assumption that the fluid remained in equilibrium with quartz. In this analysis, we relax the assumption of equilibrium with respect to quartz which requires that numerical methods be used rather than the analytical expressions obtained by Lowell, Van Cappellen, and Germanovich (1993).

We consider a single set of parallel fractures of separation d and aperture δ within which a constant and uniform upward flow occurs (fig. 3). We assume that the only reacting phase is quartz which precipitates due to the cooling of upwelling hydrothermal fluids. The fracture aperture, however, is not allowed to change in these simulations, since we are interested in describing at this stage only a single steady state. In addition, we assume that quartz completely lines the fracture walls, so that $A_{quartz} = A_{tot}$. A_{tot} is calculated from eq (59). As in the example considered by Lowell, Van Cappellen, and Germanovich (1993), we consider a steady-state system where the temperature at the top of the system (the seafloor) is 0°C. At depth, the temperature, T_1, is assumed to be 300°C. Following Lowell, Van Cappellen, and Germanovich (1993), the temperature distribution as a function of depth, $T(z)$, can be written as

$$T(z) = T_1[1 - \exp(-u_z z/\kappa)], \tag{63}$$

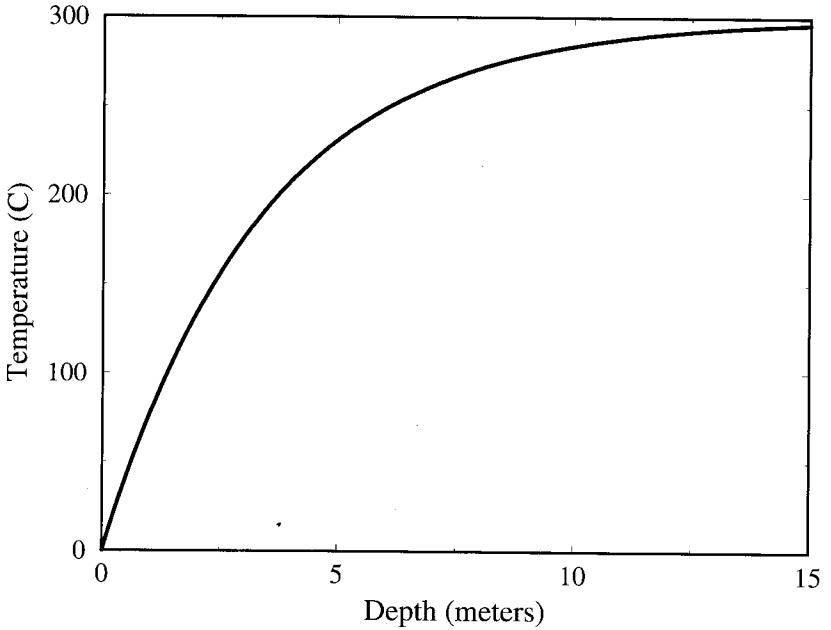

Fig. 4. Temperature versus depth below seafloor (z = 0). The seafloor is assumed to have a fixed temperature of 0°C, and at depth, below the thermal boundary layer, the temperature is 300°C. Assumes a permeability of 2×10^{-14} m^2. Calculated from eqs (63) and (64).

where u_z is the upflow Darcy flux, z is positive downward, and $\kappa = \lambda/\rho_f C_p$ is the thermal diffusivity. At high Rayleigh numbers, the temperature of the upwelling fluid remains close to 300°C, except in a thin boundary layer of thickness $l = \kappa/u$: Assuming high Rayleigh number flow (Phillips, 1991), the upward Darcy flux in the interior of the plume can be estimated from the expression

$$u_z \approx \frac{g\rho\alpha k_z T_1}{\mu}. \tag{64}$$

We use a value of 10^{-3}°C^{-1} for the thermal expansivity and a value of 2×10^{-4} Pa s for the viscosity.

As a preliminary example of the degree of supersaturation expected for a particular thermal boundary layer, consider a hydrothermal discharge zone with a permeability of 2×10^{-14} m^2. An approximate discharge velocity of 9.3 m^3 m^2 yr^{-1} is calculated from eq (64). The resulting thermal boundary layer calculated from eq (63) is about 10 m (fig. 4). The solution below the thermal boundary layer is assumed to be in equilibrium with quartz at 300°C. The temperature dependent rate constant determined by Rimstidt and Barnes (1980) is used in the

TABLE 3

Reaction rate constants at 25°C and activation energies used in the simulations

Mineral	$k_{25°C}$ (moles m^{-2} s^{-1})	Activation Energy (kJ mol^{-1})	Reference
Quartz	4.30×10^{-14}	75.0	1
K-feldspar	3.09×10^{-12}	38.2	2
Albite	3.09×10^{-12}	38.2	3
Kaolinite	2.36×10^{-14}	62.8†	4
Muscovite	2.36×10^{-14}	62.8†	5

†Activation energy assumed (Lasaga, 1984)
1. Rimstidt and Barnes (1980)
2. Helgeson, Murphy, and Aagaard (1984)
3. Chosen to be the same as K-feldspar
4. Rate from 80°C data of Nagy and others (1990)
5. Chosen to be the same as kaolinite

TABLE 4

Equilibrium constants (log Q/K) used in simulations†

	Minerals§							
Temp (°C)	0	25	60	100	150	200	250	300
Quartz	−4.61	−4.03	−3.47	−3.07	−2.73	−2.46	−2.20	−2.03
K-feldspar	−2.63	−2.51	−2.75	−3.32	−4.12	−4.79	−5.32	−6.00
Albite	0.13	−0.21	−0.97	−2.00	−3.22	−4.20	−4.97	−5.81
Kaolinite	4.92	3.17	0.89	−1.44	−3.94	−6.01	−7.79	−9.50
Muscovite	11.42	8.51	4.72	0.85	−3.28	−6.74	−9.73	−12.59
	Aqueous Complexes§§							
OH^-	14.93	13.99	13.02	12.24	11.59	11.22	11.09	11.28
CO_2(aq)	−17.20	−16.69	−16.40	−16.47	−16.95	−17.71	−18.70	−20.05
HCO_3^-	−10.62	−10.34	−10.13	−10.08	−10.22	−10.49	−10.90	−11.49
HCl(aq)	0.80	0.86	0.83	0.70	0.42	0.04	−0.48	−1.24
KCl(aq)	2.35	2.08	1.74	1.39	0.97	0.56	0.10	−0.48
NaCl(aq)	0.83	0.77	0.65	0.47	0.20	−0.11	−0.51	−1.05
NaOH(aq)	15.22	14.20	13.06	12.07	11.16	10.49	9.95	9.52
$Al(OH)^{++}$	5.69	4.93	4.10	3.50	2.65	2.13	1.75	1.34
$Al(OH)_4^-$	25.44	22.20	19.01	17.30	15.61	13.80	11.99	10.30
$H_3SiO_4^-$	10.17	9.82	9.44	9.20	9.11	9.19	9.38	9.62

† Reactions written in terms of primary species H^+, H_2O, K^+, Na^+, Al^{+++}, $SiO_{2(aq)}$, CO_3^{--}, and Cl^- in all cases as the destruction of 1 mole of the mineral or secondary species. For example, the reaction for K-feldspar would be written as $KAlSi_3O_8 + 4H^+ = K^+ + Al^{+++} + 3\,SiO_{2,aq} + 2H_2O$.

§ Thermodynamic data from Sverjensky, Hemley, and D'Angelo (1991) and Sverjensky (personal communication).

§§ Thermodynamic data from Wolery (1983).

calculation (table 3), and the thermodynamic data for quartz is given in the form of the logarithm of the equilibrium constant (table 4). A uniform grid spacing of 5 cm was used in this calculation. The effect of fluid pressure on the solubility of quartz, which is slight at temperatures below 300°C, is neglected in these calculations.

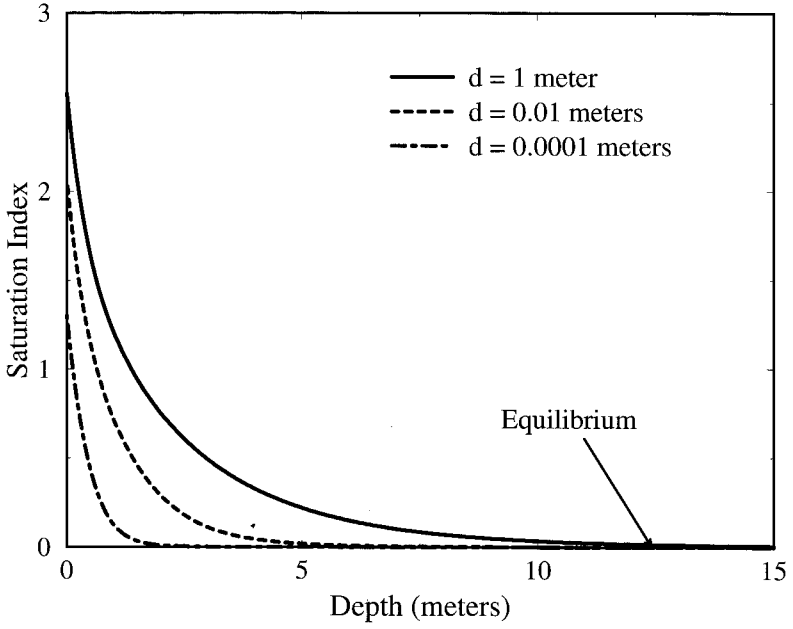

Fig. 5. Steady-state saturation indices (log Q/K) calculated for quartz using temperature profile shown in figure 4 and flow velocity calculated from eq (64). Increasing fracture spacing for a given permeability implies a decrease in surface area and thus a reduction in the effective rate constant. Note that the maximum supersaturation occurs at $z = 0$, the seafloor.

The steady-state saturation index for quartz using three different fracture spacings is shown in figure 5. Note that the greatest degree of supersaturation, as expected, occurs at $z = 0$ (that is, the seafloor, where the temperature is 0°C). Note also that as the spacing between fractures becomes smaller (that is, the fracture density, n, becomes larger), the degree of supersaturation decreases. This follows from eq (60), since in fractured rock the total surface area of rock in contact with rock increases as the number of fractures increase. From figure 5, therefore, it is apparent that the chemical kinetic behavior of silica in the fracture set depends on the spacings of the fractures in addition to the rock permeability, even though the thermal and hydrodynamic flow regimes depend only on the permeability.

The one-dimensional calculations using a temperature-dependent rate law for quartz can be used to estimate the conditions under which the local equilibrium approximation is valid for nonisothermal flow in fractures. We carried out 81 calculations of the kind shown in figure 5, systematically varying the fracture spacing, d, and the permeability, k_z. The calculations are applicable only to thermal boundary layers devel-

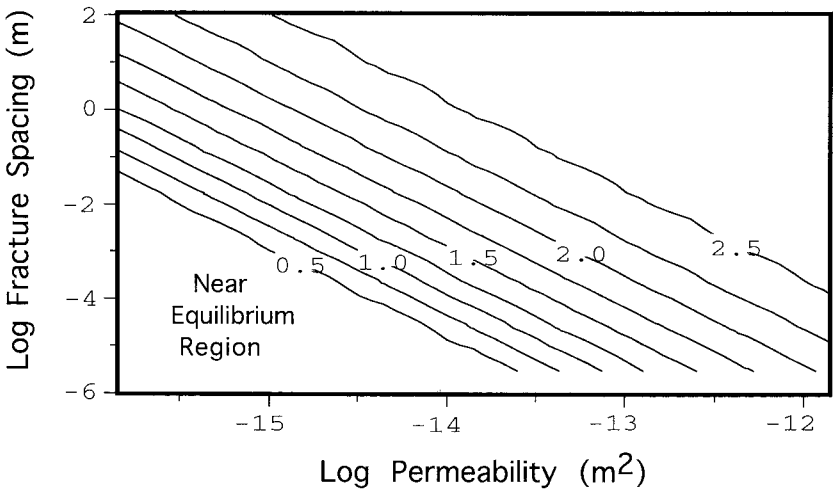

Fig. 6. Contour plot of quartz saturation indices calculated numerically at the seafloor ($z = 0$) as a function of fracture spacing and permeability. Near equilibrium conditions occur when the fractures are either finely spaced or when the permeability of the rock is low (and thus, the upward flow rates are slow). For widely spaced fractures and/or high permeabilities, the silica concentrations approach those that are in equilibrium with quartz at 300°C (the boundary condition at depth). Note the slope of the contours is ≈ -2 (see text for explanation). Based on 81 separate calculations.

oped at permeable upper surfaces and to high Rayleigh number systems, however, since it is only in this case that the flow velocities in or close to the boundary layer can be reliably estimated from eq (64). For each run, the degree of supersaturation with respect to quartz was recorded at $z = 0$ (that is, at the seafloor where the hot fluids vent) and the results contoured in figure 6.

The results of the runs indicate that the local equilibrium assumption is approximately valid in the triangular region in fracture spacing-permeability space where the quartz saturation index is less than about 0.5. As an example, the calculations predict that if a hydrothermal discharge zone were to develop above a 300°C plume in rocks having the permeability and fracture spacing estimated for the Skaergaard intrusion, the saturation index ($\log Q/K$) for quartz at the seafloor would be approx 1.25. Note that the slope of the contours in the plot is about -2, indicating that permeability (and therefore flow velocity) has a greater effect on the saturation state of the fluid than does reactive surface area. This can be explained in the following way. If the size of the thermal boundary layer is given approximately by (Lowell, Van Cappellen, and Germanovich, 1993)

$$l \approx \frac{\kappa}{u_z}, \tag{65}$$

then the Damkohler number for reactive flow in a thermal boundary layer can be written as

$$Da = \frac{k'\kappa}{u_z^2} = \frac{2k\kappa/d}{u_z^2}, \tag{66}$$

where k is the temperature-dependent reaction rate constant (in units of inverse time) averaged over the boundary layer. Eq (66) indicates that the thermal boundary layer Damkohler number depends inversely on the square of the vertical flow velocity and inversely on the fracture spacing. Since the degree of supersaturation itself depends inversely on the Damkohler number, the expression explains the slope of the saturation contours when the logarithm of the fracture spacing is plotted versus the logarithm of the permeability. The squared inverse dependence of the Damkohler number on the fluid velocity arises because the velocity affects both the rate of solute transport *and* the thickness of the thermal boundary. The physics of thermally driven flow, therefore, imposes a length scale that affects the behavior of a reactive solute.

It is often difficult to obtain reliable measurements of fluid compositions in hydrothermal systems. In many cases, the presence or absence of metastable mineral phases may give a reliable indication of what the saturation state of the solution must have been at the time of mineral deposition. Steefel and Van Cappellen (1990), for example, used the presence of metastable halloysite in weathering profiles to argue that the waters moving through the profiles could not have been at equilibrium with respect to the thermodynamically more stable kaolinite. Similarly, in hydrothermal systems, the presence of amorphous silica proves that the fluids must have been supersaturated with respect to quartz. Figure 7 is a contour plot of the saturation state of the fluid with respect to amorphous silica as a function of the fracture spacing and permeability obtained from the calculations described above. Using calculations of this kind, it may be possible to estimate permeabilities in paleo-hydrothermal systems where amorphous silica is (or was) present and where the fracture spacing can be determined.

TWO-DIMENSIONAL REACTIVE FLOW

While the one-dimensional calculations described above are useful for investigating a number of effects in nonisothermal reactive flow, a two-dimensional (at minimum) model is needed to consider the global effects of porosity and permeability change on the character of hydrothermal systems. Even in addressing the question of whether local equilibrium approximations describe a particular system, a two or three dimensional model may be necessary to represent the flow field realistically. Since we are interested at this stage in examining first order effects associated with nonisothermal reactive flow rather than in modeling a specific system, we use a relatively simple model of a single phase hydrothermal system developed in a continental setting which is broadly

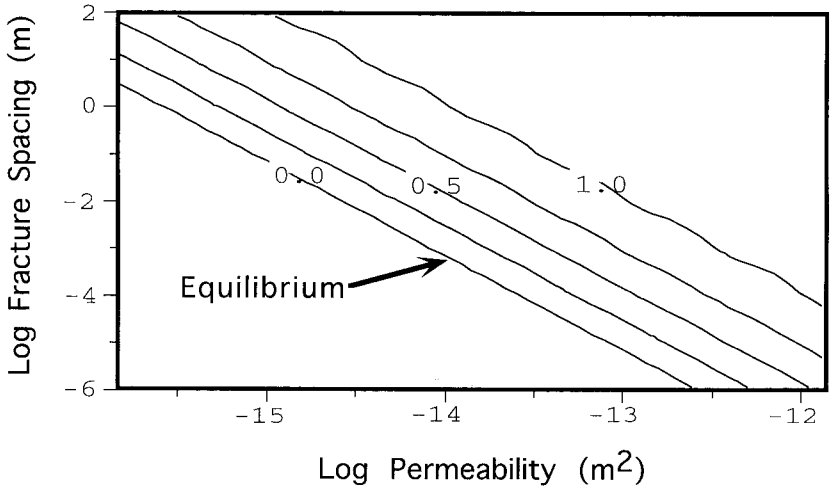

Fig. 7. Contour plot of amorphous silica saturation indices as a function of fracture spacing and permeability. Where fracture spacings can be determined, the presence or absence of amorphous silica in veins may constrain permeabilities in paleo-hydrothermal systems.

similar to many geothermal fields (for example, Yellowstone Park). The calculations are carried out using permeabilities ranging between 10^{-15} m^2 and 10^{-14} m^2, values typical of fractured igneous and metamorphic rocks (Brace, 1984; Clauser, 1992). The permeability is assumed to consist of three mutually orthogonal fracture sets, all with the same fracture spacing and aperture. We also assume that the rock is made up of a simple suite of minerals consisting of K-feldspar, albite, and quartz (a leucogranite), with the possibility that muscovite and kaolinite can form.

System description.—Consider a rectangular-shaped region of relatively permeable rock overlying a buried intrusion at depth. The bottom heated surface of the field is assumed to have a prescribed exponential temperature dependence given by

$$T = T_\infty + (T_0 - T_\infty) \exp(-10[x/l]^2), \tag{67}$$

where T_0 is 300°C at $x = 0$, T_∞ is the temperature at the base of the system one would find if a normal geothermal gradient of 25°C/km were present, and l is the half-width of the symmetric convection cell. The top boundary of the system is fixed at 50°C. The base and the top of the geothermal system are assumed to be marked by impermeable strata, thus making them no-flux boundaries. The center of the geothermal field (at x = 0) is also assumed to be a no flux boundary through symmetry (fig. 8). Finally, the vertical boundary at $x = l$ is assumed to be no-flux, which is reasonable because of the relatively short heating length prescribed by eq (67).

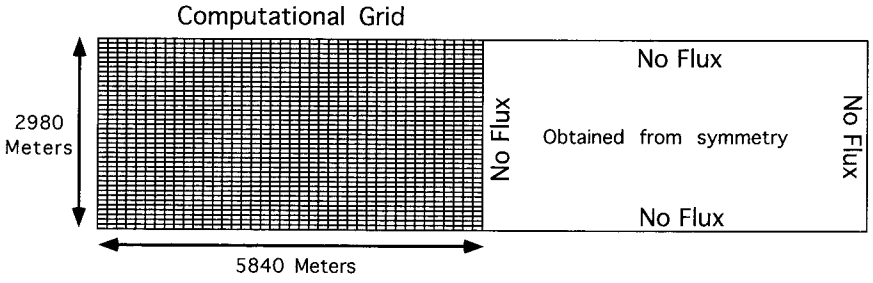

Fig. 8. Boundary conditions and computational grid used in two-dimensional calculations. The numerical calculations are carried out using 41 nodes in the x direction and 41 nodes in the z direction to discretize the half-width of the convection cell.

The actual computations are carried out on a domain measuring 2980 m deep and 5840 m wide using 1600 grid volumes (fig. 8). Distance is shown in nondimensional form, obtained by scaling depth by the total depth of the system, h, and horizontal distance by the half-width of the system, l. This results in a uniform spacing of 74.5 m in the vertical dimension and 146 m in the horizontal dimension.

Equilibrium and kinetic database.—Equilibrium constants for the heterogeneous and homogeneous reactions are calculated at each grid point using a fifth order polynomial fit to the data in table 4. The log K's for the minerals are taken from Sverjensky, Hemley, and D'Angelo (1991) who derived them from Berman (1988). The log K's for the complexation reactions are taken from the EQ3/EQ6 database (Wolery and others, 1990). Activity coefficients are calculated from an extended Debye-Huckel formulation (Wolery, 1983). The pressure dependence of the solubilities is neglected.

The rate data used in the calculations are given in table 3 and are calculated from eq (31). Eq (29) gives the form of the rate law used in all the calculations with both $\mathcal{M}$ and $n = 1$ and with $p = 0$ (that is, "first-order" kinetics and no inhibitory or catalytic effects).

Initial conditions.—We assume that the geothermal field begins with a normal geothermal gradient of 25°C/km and that the sudden intrusion of a magma body at depth causes the lower impermeable boundary to be heated instantaneously at $t = 0$. To complete the specification of the initial conditions, we need to give the initial total concentrations of the solutes or the mineral equilibria used to constrain the concentrations (table 5) and the initial (or primary) modal mineralogy of the rock. We restrict ourselves here to the chemical system of KCl, NaCl, Al_2O_3, SiO_2, and H_2O. Since the initial fluid is not isothermal, the use of a mineral constraint results in differing initial concentrations which depend on the local temperature.

It is important to point out that the choice of boundary and initial conditions can have a significant effect on the behavior of the system. The

TABLE 5

Total solute concentrations and mineral constraints used in the initial fluid

Element	Concentration†	Constraint
K^+		K-feldspar
Na^+	10^{-3}	
SiO_2		Quartz
CO_2	10^{-4}	
Al^{+++}		Albite
H^+		Muscovite
Cl^-		Charge balance

†Total concentration in moles kg^{-1}

results given below, therefore, would be very different if, for instance, an influx of reactive fluid (for example, meteoric groundwater or magmatic water) occurred across one of the boundaries.

Steady-state reactive convection.—Before proceeding to simulations in which the precipitation and dissolution reactions are allowed to affect the rock's porosity and permeability, we carry out a number of calculations in which there is no feedback between the two. This allows us to identify those effects that can be directly attributed to porosity-permeability change and those that result from other processes occurring in the model geothermal field. Steady-state temperature fields and streamlines for permeabilities of 10^{-15}, 5×10^{-15}, and 10^{-14} m^2 (corresponding to Rayleigh numbers of 50, 250, and 500 using the parameters listed in table 2) are shown in figure 9. The porosity in these simulations is assumed to be 0.05 percent, yielding the fracture spacings and total surface areas given in table 6. At a permeability of 10^{-15} m^2, the temperature contours show only a slight disturbance from those expected for purely conductive heat transfer. Nonetheless, convection develops because of the presence of the distributed heat source at depth. With increasing permeability (and Rayleigh number), the flow velocities in the upwelling plume become larger as indicated by the closeness of the spacing between the streamlines. At a permeability of 10^{-14} m^2, for instance, the convection cell is characterized by a broad recharge zone and a relatively narrow upwelling zone with higher flow velocities. This results in the formation of a nearly isothermal plume of about 225°C in the interior portions of the convection cell and the development of a thermal boundary layer at the top and bottom of the system.

Steady-state quartz reaction rates and supersaturation indices (log Q/K) are shown in figure 10 for the calculations using permeabilities of 10^{-15}, 5×10^{-15}, and 10^{-14} m^2. The reaction rate for quartz is in units of volume percent my^{-1}. Positive values of the reaction rate indicate precipitation, whereas negative values indicate dissolution. As expected, quartz dissolves in the region where fluids move up a temperature gradient close to the heat source at depth and precipitate within the cooling plume. With increasing Rayleigh number, however, precipitation tends

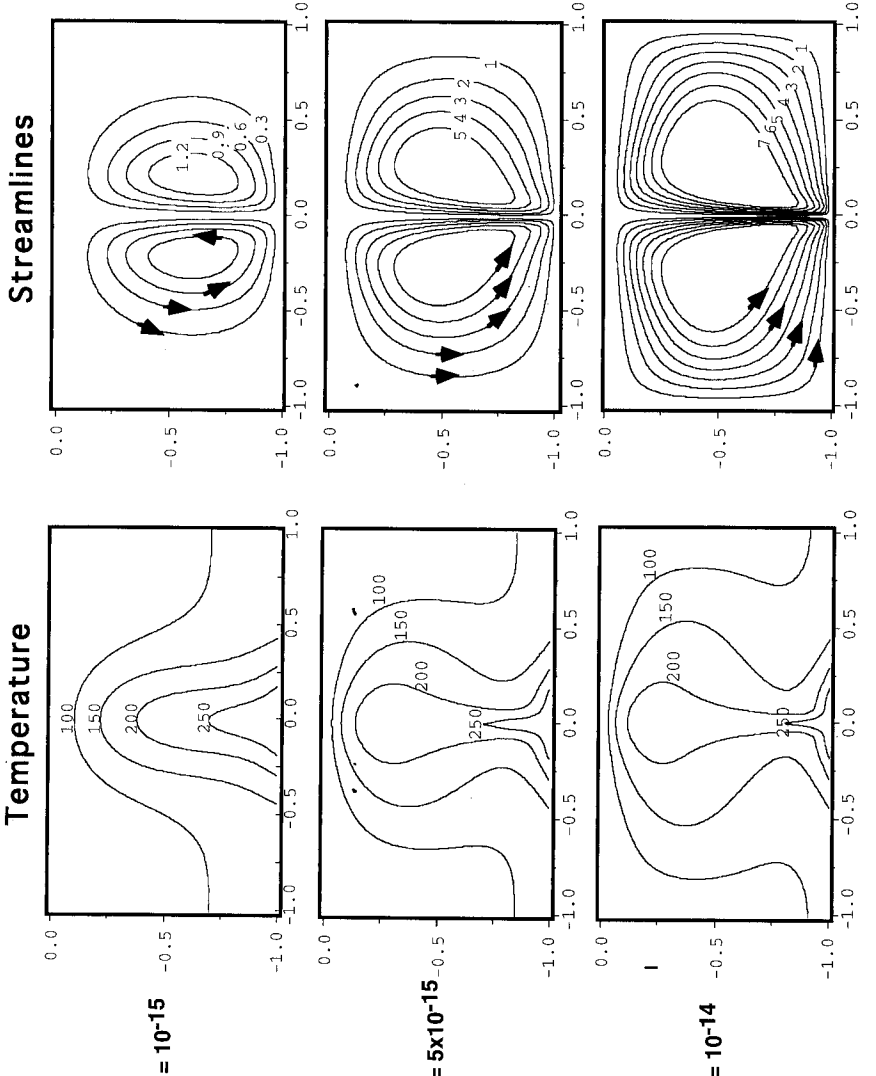

Fig. 9. Isotherms (°C) and streamlines in steady-state hydrothermal convection cell for permeabilities of 10^{-15} m^2, 5×10^{-15} m^2, and 10^{-14} m^2 (Rayleigh numbers of 50, 250, and 500). Depth and horizontal distance are non-dimensional. No porosity-permeability feedback between reactions and flow regime. Streamlines in units of κ (table 2).

TABLE 6

Parameters used in two-dimensional calculations

Permeability (m^2)	Rayleigh Number	Porosity (%)	Fracture Spacing (m)	Fracture Aperture (μm)	Surface Area (m^2)
10^{-15}	50	0.05	0.05	8.5	117
5×10^{-15}	250	0.05	0.11	19	53
10^{-14}	500	0.05	0.16	27	37

to focus in the thermal boundary layer at the top of the system and close to the thermal maximum at the base of the system where the solubility decrease between 300° and 250°C is the greatest. The gap in the quartz precipitation contours which develops between the two precipitation zones corresponds to the nearly isothermal interior portion of the plume which forms in the higher permeability simulations.

As indicated by the one-dimensional calculations described above, the greatest supersaturation with respect to quartz occurs in the thermal boundary at the top of the system. Even though in the calculation using permeabilities of 5×10^{-15} and 10^{-14} m^2, the quartz precipitation rates are greater near the base of the system than they are at the top, the large quartz reaction rate constant at temperatures between 250° and 300°C ensures that close to equilibrium conditions prevail at depth. Note that the predicted supersaturations with respect to quartz are less than those calculated by the one-dimensional calculations described above. This is primarily due to the fact that the flow velocities near the upper impermeable surface are significantly less than those predicted by the analytical expression in eq (64). In the simulations using a permeability of 10^{-14} m^2, for example, the Darcy flux close to the top of the system is about 0.1 m^3 m^{-2} yr^{-1} according to the numerical calculations. As discussed above, eq (64) applies to the interior portions of plume, far from any impermeable surface. As a result, the thermal boundary layer is not as narrow in the two-dimensional calculations as would be predicted using eqs (64) and (63).

The two-dimensional calculations suggest that a local equilibrium approximation would be justified for the particular conditions used in the simulation, with the exception of the region corresponding to the thermal boundary layer which develops in the calculations using high permeabilities. Even in the calculation using a permeability of 10^{-14} m^2, however, the supersaturation with respect to quartz is modest because of the decrease in flow velocities close to the impermeable upper surface. The conclusion that the local equilibrium approximation is justified, therefore, does not apply in the case of a permeable upper surface, where the larger supersaturations are more accurately predicted by the one-dimensional simulations described above. In the nearly isothermal high temperature core of the plume, the fluid remains everywhere very close to equilibrium with respect to quartz (and the other primary minerals

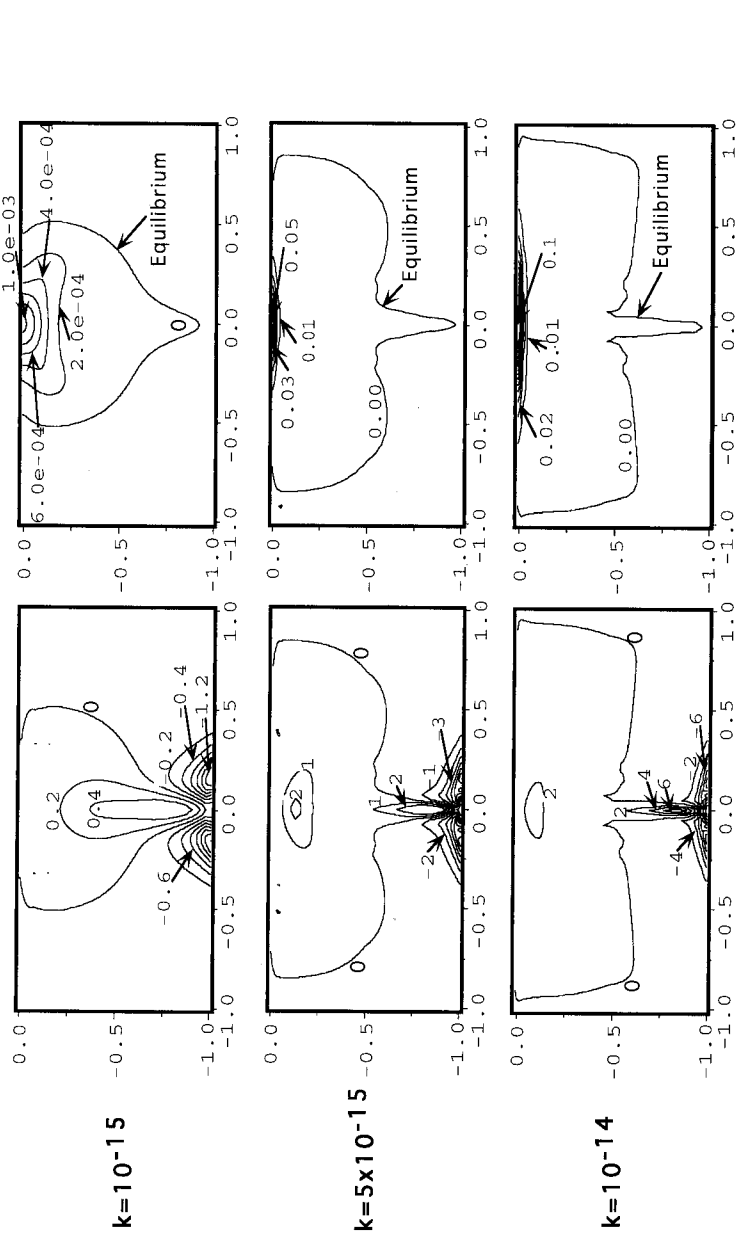

Fig. 10. Steady state quartz reaction rates (volume percent my^{-1}) and quartz supersaturation indices (log Q/K) for calculations using permeabilities of 10^{-15}, 5×10^{-15}, and 10^{-14} m^2. Largest reaction rates occur in the highest temperature portion of the system near the lower boundary. Highest supersaturations develop in the cool thermal boundary layer at the top of the system. Note that at a permeability of 10^{-15} m^2, the calculations suggest that the local equilibrium assumption would be fully justified for this particular system.

present, albite and K-feldspar). Significant departures from equilibrium in the high temperature isothermal core are expected only where the spacing between fractures becomes very wide for a given permeability or where the flow rates themselves become extremely rapid. Note that where temperature gradients are linear or approximately so (implying low Rayleigh number convection), in contrast to the conclusions of Wells and Ghiorso (1991), significant departures from equilibrium are unlikely without extremely widely spaced fractures.

The steady state precipitation rate for K-feldspar and the dissolution rate for albite, obtained from the same calculations used for the quartz reaction rates, are shown in figure 11. Note the strong similarity between the K-feldspar precipitation rates and the albite dissolution rates, indicating a nearly mole for mole replacement of albite by K-feldspar which conserves H^+, Al, and SiO_2. Contour plots of the rates of albite precipitation and the dissolution rate of K-feldspar show a similar mole for mole replacement of K-feldspar by albite in the regions where the fluid moves up a temperature gradient. The solution pH (fig. 12) is buffered by the K-feldspar-albite reaction at the ambient temperature, thus producing contours that mimic the temperature contours very closely. Muscovite and kaolinite don't form in significant quantities in any of the simulations.

The albite-K-feldspar reaction, because it involves a nearly mole for mole replacement, produces almost no net change in the porosity of the rock. The porosity change which occurs is due to the mobility of silica resulting from the temperature-dependence of quartz. In this simple system, therefore, we expect that the rates of porosity increase and decrease will show a topology within the model geothermal field which is very similar to the quartz reaction rate topologies. Figure 13 shows the instantaneous rate of porosity change predicted from the calculations. The units of the contours are percent porosity per million years. In this case, we compute a rate of porosity change using eq (33) (that is, by summing the volume percent of the various minerals in the system) even though the porosity is *not updated* in the reactive transport calculations. Physically, one could view this as corresponding to a case where the local dilation or closing of a fracture due to other effects like fluid pressure balances the change in fracture aperture due to precipitation or dissolution. The rate of porosity change shown in figure 13, therefore, is the change due solely to precipitation and dissolution reactions.

Fracture porosity represents a bulk property that may be difficult to estimate easily in the field. We can calculate the predicted rates of fracture aperture change directly using eq (53), thus providing information more easily observed by the field geologist. The rates of aperture change depend on the fracture spacing in the particular system, however, so the observation of fracture apertures must always be done in conjunction with observations on the fracture spacing in the rock (Norton and Knapp, 1977; Manning and Bird, 1991). Figure 14 shows the rate of aperture change in microns per million years predicted for the 3

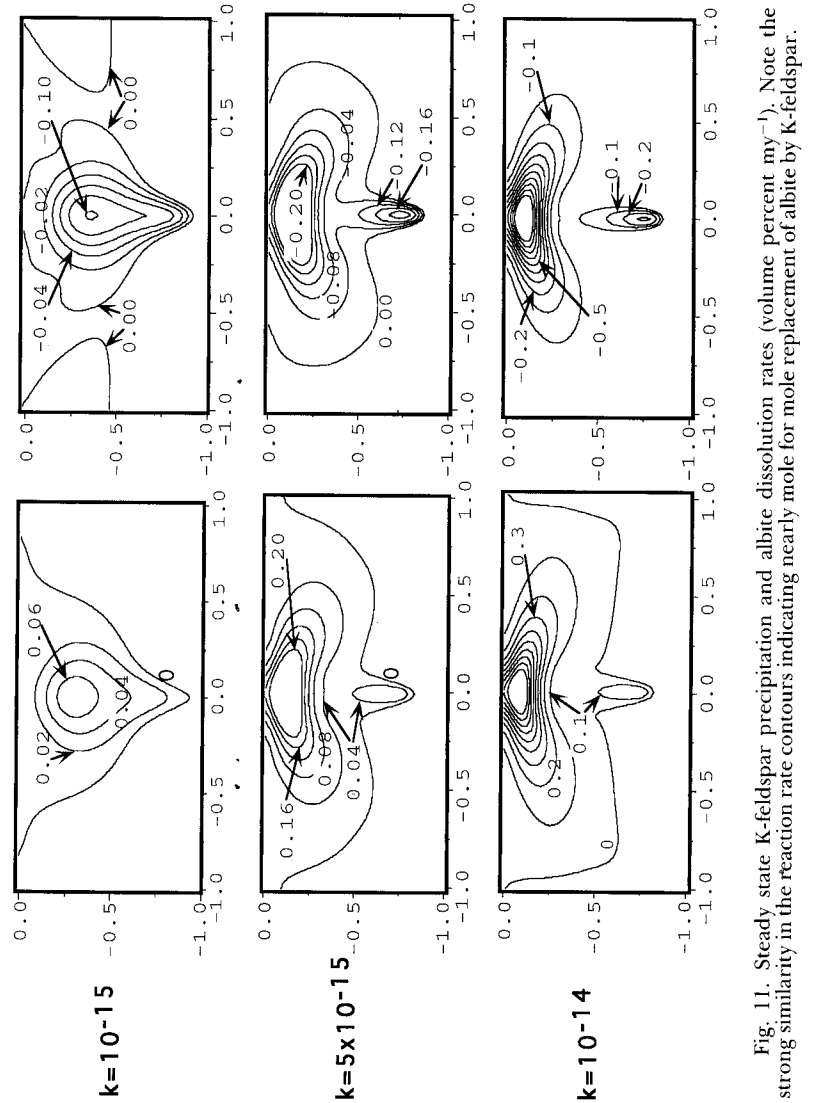

Fig. 11. Steady state K-feldspar precipitation and albite dissolution rates (volume percent my^{-1}). Note the strong similarity in the reaction rate contours indicating nearly mole for mole replacement of albite by K-feldspar.

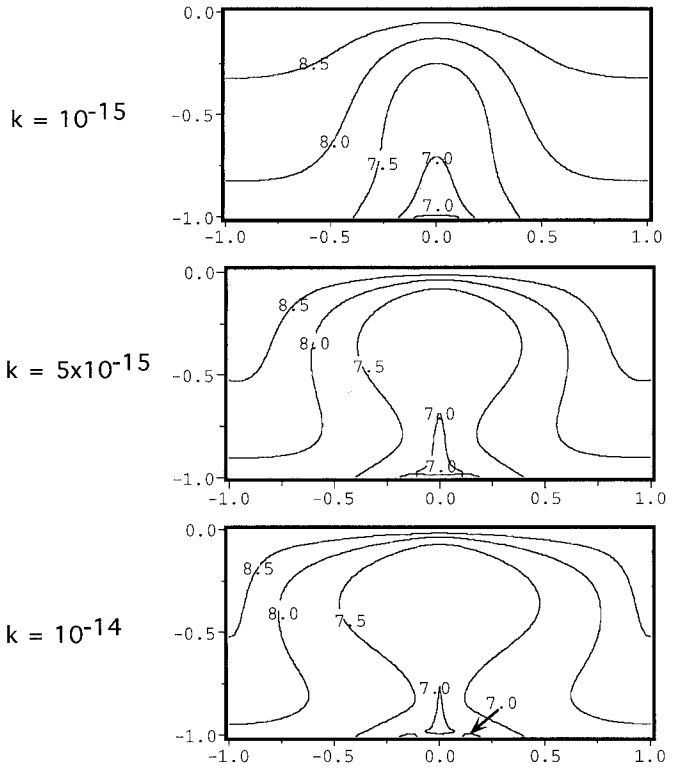

Fig. 12. Steady state solution pH in convection cell.

simulations. From figures 13 and 14 we can see that if fracture dilation or closing due to fluid pressure effects does not occur, the convection process will eventually produce a region of reduced permeability in the upwelling portions of the system where cooling causes quartz to precipitate and an enhancement of the permeability in the regions close to the heat source at depth where fluids move up temperature. In the next section, we examine the feedback between hydrodynamic flow, heat transfer, and chemical reactions which arise due to reaction-induced porosity and permeability change.

REACTION-INDUCED POROSITY-PERMEABILITY CHANGE

In this section we couple the porosity and permeability of the evolving geothermal field to the reactions taking place in the rock. This requires that a fully transient calculation be carried out, since one of the questions to be addressed by the calculation is whether the thermally driven convection process ever attains a steady state when reactions can affect the rock's permeability. We use here a permeability of 10^{-15} m^2 and

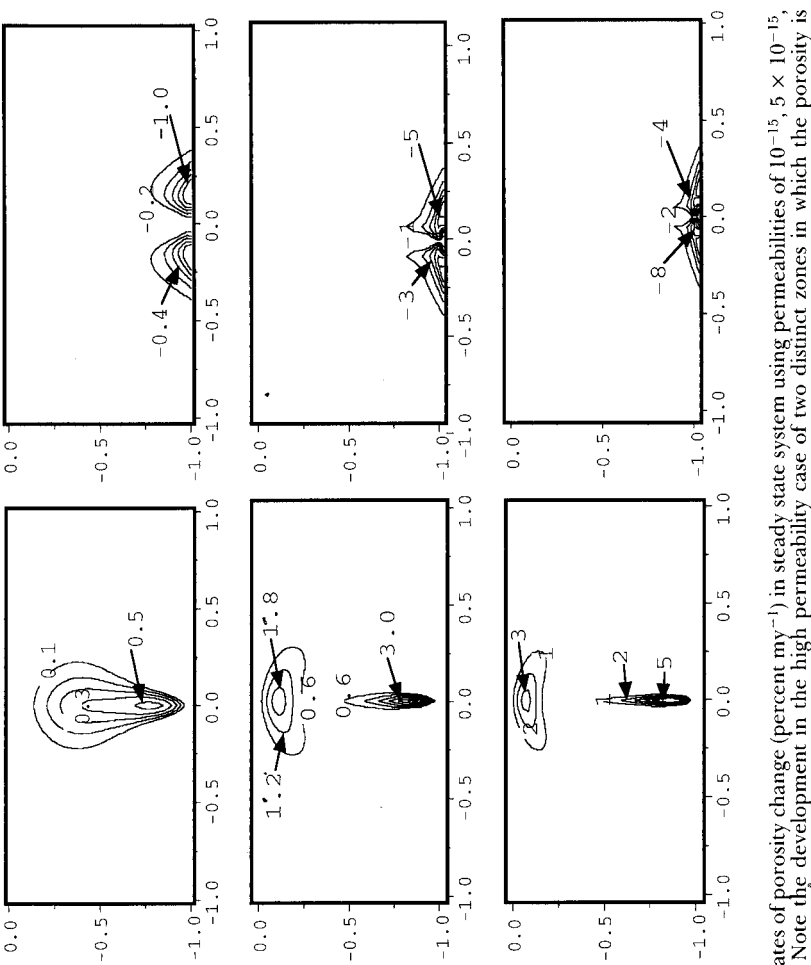

Fig. 13. Rates of porosity change (percent my^{-1}) in steady state system using permeabilities of 10^{-15}, 5×10^{-15}, and 10^{-14} m^2. Note the development in the high permeability case of two distinct zones in which the porosity is reduced: in the high temperature portion of the plume close to the bottom boundary and in the thermal boundary layer at the top of the system. Calculation does not include a porosity-permeability feedback into the transport.

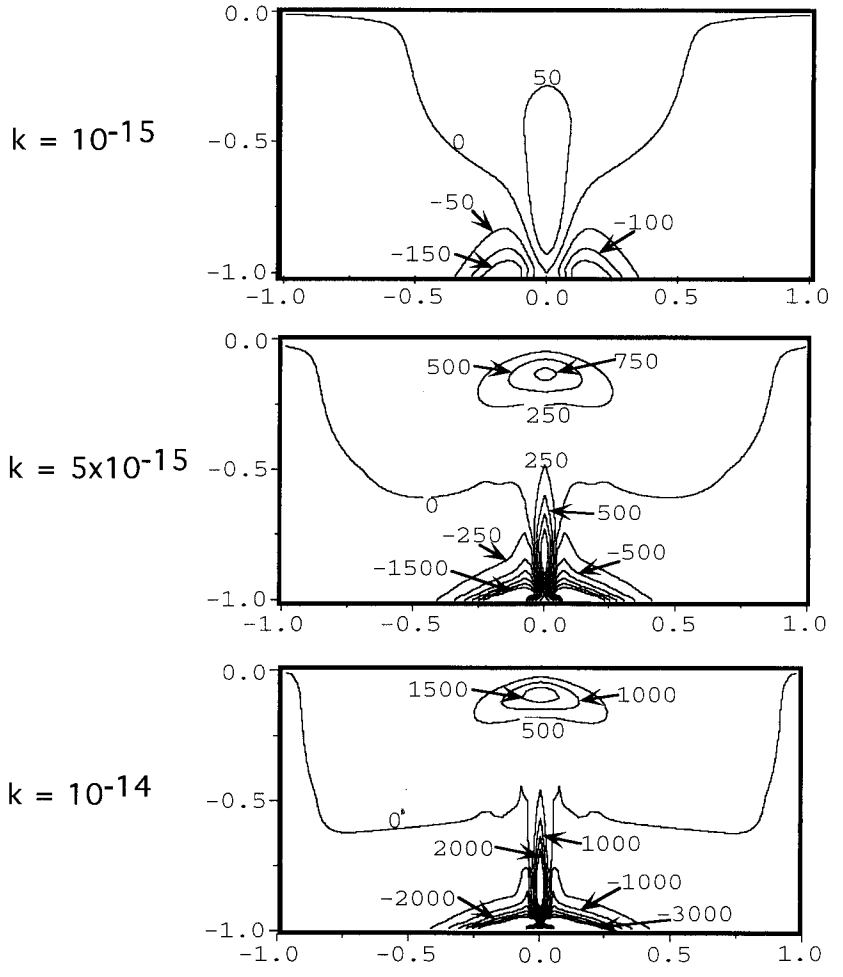

Fig. 14. Rates of change of the fracture apertures (μm my^{-1}) at steady state. Calculation does not include a feedback into permeability.

a fracture spacing of 0.05 m, corresponding to a rock such as that surrounding the Skaergaard intrusion in Greenland (Norton and Taylor, 1979; Manning and Bird, 1991). The physical system as described above, however, bears no other similarity to the Skaergaard, which is used only to provide what may be a reasonable porosity-permeability relationship. All other features of our model geothermal field are the same as those in the steady state calculations described above in which the porosity and permeability of the rock were not allowed to change.

As pointed out by Budi Sagar (personal communication), the presence of no-flux boundaries can have a significant effect on the dynamical

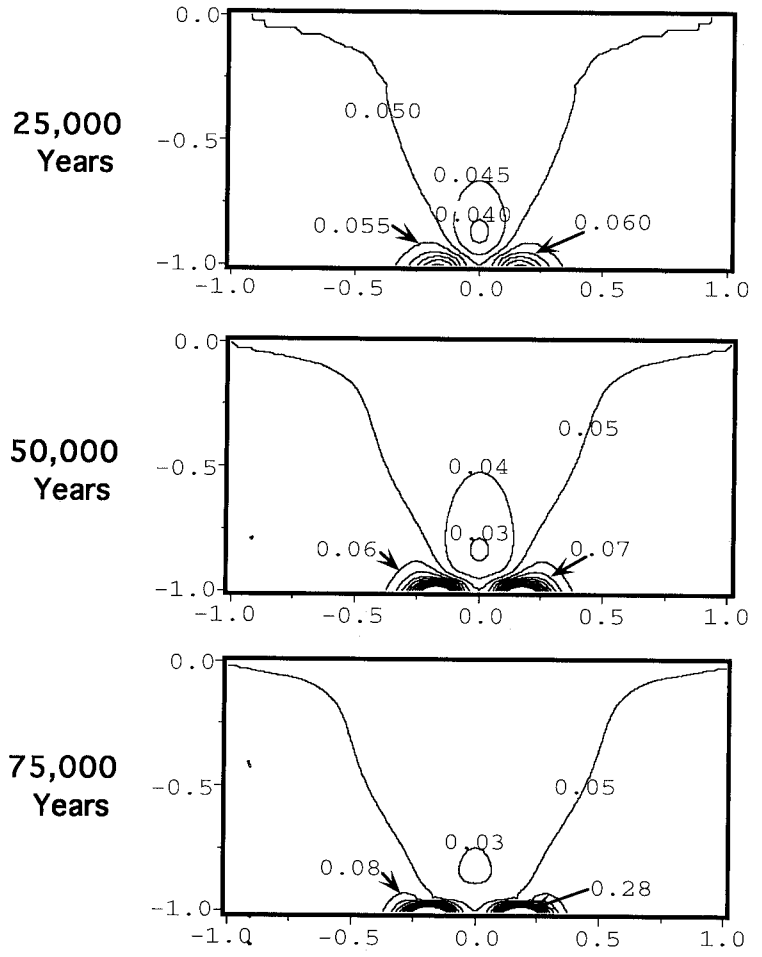

Fig. 15. Fracture porosity (percent) at 25,000, 50,000, and 75,000 yrs for an initial permeability of 10^{-15} m^2 (Ra = 50) and for the case in which the porosity and permeability are allowed to change with time due to precipitation and dissolution reactions. Note the intensification of the high porosity zone with time resulting from the reactive infiltration instability.

behavior of the system when reaction-induced permeability changes occur. The no-flux boundary, or equivalently any interface where a large change in permeability occurs, may become the focus of the greatest permeability changes.

Figure 15 shows the time evolution of the fracture porosity out to 75,000 yrs. At 25,000 yrs, the fracture porosities show a topology similar to the topology shown by the instantaneous rates of porosity and aperture change in the calculations without porosity-permeability feedback (fig. 13 and 14). At 25,000 yrs, the smallest fracture apertures occur at

depth in the upwelling plume where the fluid cools from about 300° to 225°C. The largest apertures occur immediately adjacent to the lower boundary where the flow moves up the sharpest temperature gradient. In the terminology of Phillips (1991), this region corresponds to the most negative value of the Rock Alteration Index, described by

$$RAI = \mathbf{u} \cdot \nabla T. \tag{68}$$

With increasing time, however, the topology and the rate of change of the fracture porosity evolves significantly due to the feedbacks between the reaction-induced permeability change and the flow and temperature regime. By 50,000 yrs, the maximum fracture porosity is approx 0.1 percent at the base of the system, a change of about 0.06 percent from its initial value, while the minimum fracture porosity shows a change of only about 0.03 percent (fig. 15). The effect is even more pronounced by 75,000 yrs when the maximum fracture porosities are about 0.28 percent along the bottom boundary. Similar effects can be seen in contour plots of fracture aperture and permeability (fig. 16). By 75,000 yrs, the minimum permeability in the upwelling plume is about 1.5×10^{-16} m^2 while the permeability has increased to as much as 2.5×10^{-13} m^2 where the fluid flows up temperature near the base of the system. As discussed above, if the initial permeability in the system had decreased gradually with depth, the region in which permeability enhancement occurs would be more diffuse. The presence of the no-flux boundary at depth, therefore, results in a more rapid channelization of the flow due to reaction-induced permeability changes than would, for example, an exponentially decreasing permeability with depth.

The changes in permeability resulting from the precipitation and dissolution reactions have a significant effect on the flow and temperature regime (fig. 17). At 25,000 yrs, the temperature field is topologically similar to that shown in figure 9, although it has not yet evolved to a steady state. With increasing time, however, the shape of the isotherms begins to change significantly due to the modification of the flow field resulting from the permeability change. These effects of the permeability change can be seen clearly in the contour plots of the stream function (fig. 17). At 25,000 yrs, the convection cell is broadly similar to the steady state configuration in figure 9. The enhancement of the permeability along the lower boundary due to the dissolution of quartz results in a focusing of the flow in that region. In contrast, the reduction in permeability in the plume causes the flow to diverge around the low permeability zone. By 75,000 yrs, relatively little flow moves up through the low permeability zone in the center of the system. The divergence of the upwelling flow away from this low permeability zone explains the unusual shape of the isotherms in the plume at 75,000 yrs (fig. 17).

The behavior described above is the result of the reactive infiltration instability described by Ortoleva and others (1987) and by Steefel and Lasaga (1990). The regions of enhanced porosity and permeability tend to capture more flow which has the effect of accelerating the rate at which

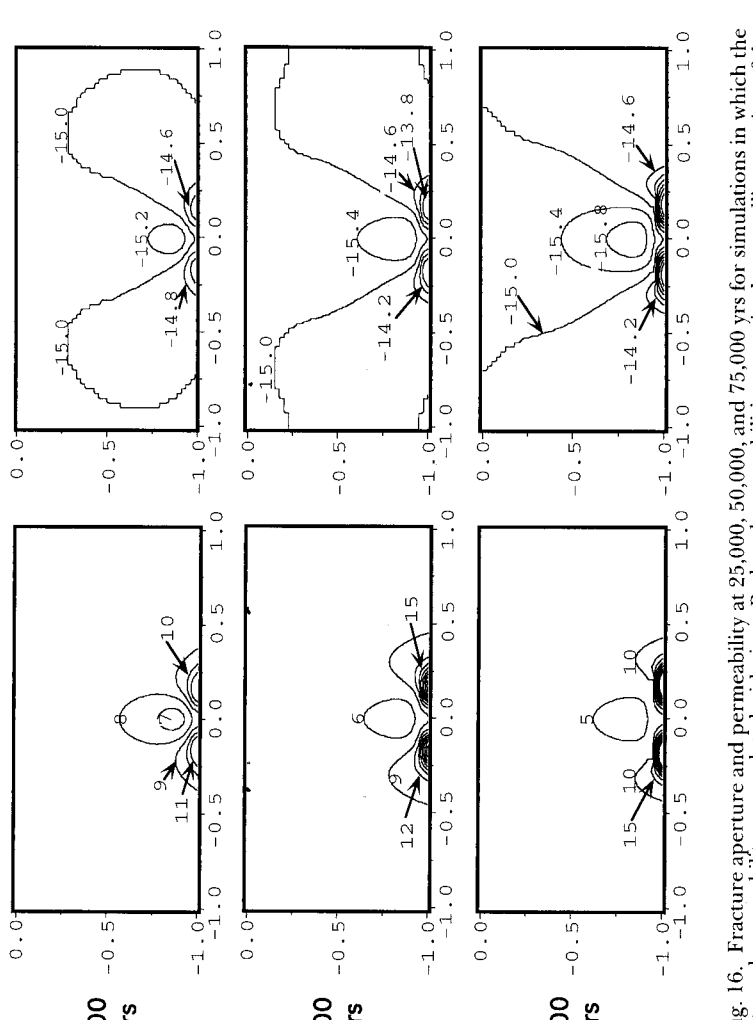

Fig. 16. Fracture aperture and permeability at 25,000, 50,000, and 75,000 yrs for simulations in which the porosity and permeability are updated with time. Reduced permeabilities occur in the upwelling portion of the plume where the precipitation of quartz reduces the fracture apertures. Strong increases in permeability occur where the fluid moves up temperature near the heat source at depth.

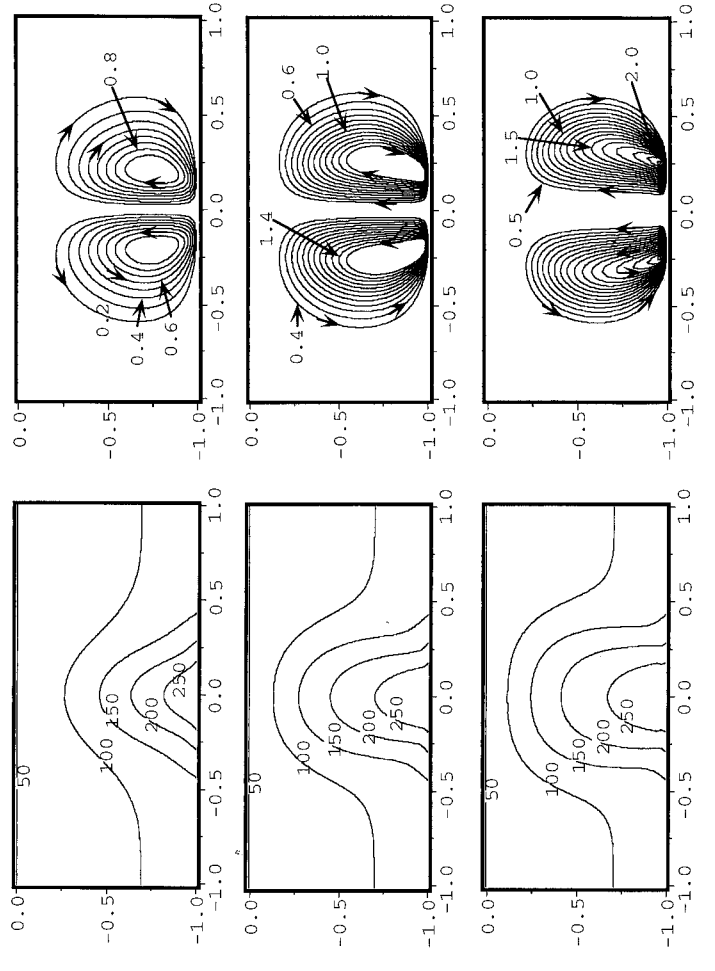

Fig. 17. Time evolution of isotherms and streamlines (units of κ) for case in which the reactions and flow regime are coupled through the permeability. Note the development of channelized flow at 50,000 and 75,000 yrs at depth where dissolution reactions have increased the permeability of the rock. The low velocities in the center of the system where the ascending fluids cool is due to the reduction in permeability resulting from quartz precipitation.

the transport-limited reactions proceed. The positive feedback between the rate of flow and the rate of reaction where a permeability increase occurs results, therefore, in an instability. In contrast, where precipitation reduces the permeability of the rock, it also reduces the rate of flow through that region. In this case, the overall reaction rate, which is limited by the rate at which silica-rich fluids are provided by higher temperature regions, decelerates with time. Note that in contrast to the isothermal case considered by Ortoleva and others (1987) and by Steefel and Lasaga (1990), these effects do not depend on any particular concentration boundary condition. They result purely from the imposed temperature gradients in the system and in fact are an inevitable consequence of the convection process unless other processes act to reverse the effects.

Simulations in which the initial permeability was 5×10^{-15} and 10^{-14} m^2 show behavior similar to the case where the initial permeability was assumed to be 10^{-14} m^2, although the entire process occurs much more rapidly. At an initial permeability of 10^{-14} m^2, for example, the flow and temperature field is substantially modified by as little as 15,000 yrs after the appearance of the heat source at depth. These results, along with the results of the simulations carried out using a permeability of 10^{-15} m^2, indicate that reaction-induced permeability change is likely to have a significant effect on the character of a crustal hydrothermal system. It appears that for a system with a porosity-permeability structure such as might be commonly found in both continental and marine settings, the time scale for significant permeability change is less than the time required to achieve a hydrodynamic and thermal steady state. The calculations presented here suggest that the effect of reaction-induced permeability changes is potentially profound and needs to be considered carefully in future simulations of hydrothermal systems.

CONCLUSIONS

We have presented a quantitative model that couples chemical reactions, multi-species chemical transport, hydrodynamic flow, and heat transfer in one and two dimensions. The model is based on a new algorithm which simultaneously solves for multi-species transport and reaction and which includes kinetic-based formulations of mineral-water reactions. Most importantly, the model can be used to investigate crustal flow systems where multi-component reaction and transport are important and where closed system modeling may not be applicable.

The one and two-dimensional reactive transport model has been applied to two important problems related to reactive flow in hydrothermal systems. The model was used to determine whether it is likely that the local equilibrium approximation is valid in hydrothermal systems. The calculations indicate that the saturation state of the fluids in a fractured rock depends on its bulk permeability, which determines the flow velocities, and the spacing of fractures, which for a given porosity and permeability determines the aperture of the fractures. The results of

one-dimensional calculations applicable to high Rayleigh number flow in systems with permeable upper boundaries indicate that significant disequilibrium with respect to silicate phases may occur in the low temperature thermal boundary layers. We have shown that the degree of supersaturation in the boundary layers depends inversely on the fracture spacing (and thus on the fracture aperture) and inversely on the square of the upward flow velocity. The squared dependence on the flow velocity arises because of its effect on both the rate of solute transport and on the thickness of the thermal boundary layer. In systems with impermeable upper surfaces, the calculated disequilibria is less because of the decrease in flow velocities near the upper boundary. For permeabilities as high as 10^{-14} m^2 in systems with an impermeable upper surface, the local equilibrium approximation appears to be reasonable unless the fractures are widely spaced (for example, >100 m). All the calculations indicate that where the flow is sufficiently slow that the temperature profile is linear, the local equilibrium approximation is good unless the fractures are extremely widely spaced.

The model has also been used to study the effects of reaction-induced porosity and permeability change on the character of the convective regime. Using a porosity-permeability relationship such as that observed for the Skaergaard intrusion, the calculations indicate that reaction-induced permeability change will prevent the convection cell from attaining a hydrodynamic or thermal steady state. We have shown that the reactive infiltration instability of Ortoleva and others (1987) operates in nonisothermal flow systems where the effect is independent of any particular concentration boundary condition. Permeability reduction, which typically occurs in the upwelling portion of the convection cell, will cause the plume to become increasingly diffuse with time as the ascending fluids diverge around the cemented zone. Permeability enhancement, which most commonly occurs where fluids move up temperature, can result in channeling of flow.

ACKNOWLEDGMENTS

Acknowledgment is made to the Branch of Energy Science of the Department of Energy (DE-FG02-90-ER14153), to the Donors of the Petroleum Research Fund, administered by the American Chemical Society, (PRF 22364-AC2), and to U.S. National Science Foundation (EAR-9017976) for the support of this research. We are grateful for the constructive reviews of the manuscript by Jeff Raffensperger, Owen Phillips, and Grant Garven.

APPENDIX I

Solution method for reaction-transport equation

Newton's method.—Newton's method solves a set of nonlinear equations by making use of a Taylor series expansion around a function f(x) to linearize the problem. Letting **ln C** denote the entire vector of values of the logarithms of the concentrations which must be

solved for, then in the neighborhood of **ln C** the functions f_i can be expanded (Press and others, 1986)

$$f_i(\mathbf{ln\ C} + \delta\ \mathbf{ln\ C}) = f_i(\mathbf{ln\ C}) + \sum_{j=1}^{N_c \times M} \frac{\partial f_i}{\partial\ ln\ C_j}\, \delta\ ln\ C_j + O(\delta\ \mathbf{ln\ C}^2) \tag{A-1}$$

where $O(\delta\ \mathbf{ln\ C}^2)$ refers to all terms of second order and higher. If we neglect these second order and higher terms, then we can move toward the roots of all the f_i simultaneously by solving a set of linear equations for the corrections $\delta\ \mathbf{ln\ C}$. This means that each iteration making use of the Taylor series expansion can be written as

$$\sum_{j=1}^{N_c \times M} \frac{\partial f_i}{\partial\ ln\ C_j}\, \delta\ ln\ C_j = -f_i. \tag{A-2}$$

Note that if we define the f_i as making up the elements of the vector **b** and the $\partial f_i / \partial\ ln\ C_j$ as forming the elements of the matrix **A** (referred to as the *Jacobian* matrix), then eq (A-2) can be written in the familiar form

$$\mathbf{A} \cdot \delta\ \mathbf{ln\ C} = \mathbf{b}. \tag{A-3}$$

Once the $\delta\ ln\ C_j$ are computed, they are used to update the concentrations of the primary species

$$ln\ C_j^{new} = ln\ C_j^{old} + \delta\ ln\ C_j \qquad (i = 1, \ldots, N_c \times M). \tag{A-4}$$

Structure of the Jacobian matrix.—It is instructive to examine the structure of the Jacobian matrix which arises from the discretization of the coupled reaction-transport equations, since it will have a bearing on the choice of a method to solve the set of linear equations given by eq (43). The Jacobian matrices exhibit a *block tridiagonal* structure in the case of one dimensional transport. The blocks making up the matrix **A** are N_c by N_c submatrices corresponding to the primary species at any grid point. That is, if we are writing the conservation equation for $SiO_{2,aq}$ at a particular point in space, the equation $f_{SiO_{2,aq}}$ will be differentiated with respect to all N_c primary species (for example, $SiO_{2,aq}$, Al^{+++}, K^+, et cetera). As an example, consider a one-dimensional system described by 4 primary species which is discretized using 4 grid points. The matrix **A** can be represented compactly as a series of 4×4 submatrices, $\mathbf{A}_{ij}$, such that

$$\mathbf{A} = \begin{bmatrix} \mathbf{A_{11}} & \mathbf{A_{12}} & 0 & 0 \\ \mathbf{A_{21}} & \mathbf{A_{22}} & \mathbf{A_{23}} & 0 \\ 0 & \mathbf{A_{32}} & \mathbf{A_{33}} & \mathbf{A_{34}} \\ 0 & 0 & \mathbf{A_{43}} & \mathbf{A_{44}} \end{bmatrix} \tag{A-5}$$

Those readers with some familiarity with numerical methods will recognize that this is the structure of any finite difference formulation of a partial differential equation (for example, the conservation of energy equation), except that in this case the entries are submatrices rather than single coefficients. If we reduced the system to a single chemical component, then the forms of the temperature and reaction-transport matrices would be identical. The submatrices need not be filled entirely with non-zero elements, but, in general, they will be dense in systems with either a large number of minerals or a great deal of complexation. The diagonal submatrices ($\mathbf{A_{11}}$, $\mathbf{A_{22}}$ et cetera) contain contributions from both the heterogeneous reaction term, R_j^{min}, and from the total soluble concentrations (the U_j's). The offdiagonal submatrices, in contrast, contain only contributions from the total

soluble concentrations at the neighboring grid points. Note that the matrix **A** is sparse (that is, the ratio of zero to non-zero entries in the matrix is large) when the number of grid points is large (for example, greater than 100), even though the submatrices (reflecting the coupling between the various species due to reactions) may themselves be fairly dense.

Solution method.—Any method used to solve the set of equations described by eq (43) should take into account both the sparseness of the Jacobian matrix **A** and its block structure resulting from the finite difference formulation. Direct methods of matrix inversion that don't take advantage of the sparseness of the matrix work poorly because the elimination procedure tends to produce many non-zero entries in the off-diagonal positions. Potentially the most powerful methods, particularly for one-dimensional problems, are exact methods that take advantage of the tridiagonal structure of the Jacobian matrix (Oran and Boris, 1987; Golub and Van Loan, 1989). In simulations in which there is strong coupling between diagonal and off-diagonal matrix components, the iterative methods become increasingly less efficient relative to the exact block tridiagonal solvers. The increased coupling occurs when the transport terms are large given a particular discretization. The exact block tridiagonal solvers may be extended to two-dimensional problems with the use of an *alternating direction implicit* or ADI method (Press and others, 1986).

Iterative methods are another common way of solving large, sparse systems of linear equations. Their advantage is that they minimize both the number of necessary operations and the amount of computer storage required (Ortega and Rheinboldt, 1970, Stoer and Bulirsch, 1980). It is a straightforward procedure, for instance, to store a $N_c \times M$ by $N_c \times M$ Jacobian matrix arising from discretization of a one dimensional problem as a $N_c \times 3$ by $N_c \times M$ rectangular matrix. The methods are also less subject to the problems associated with the accumulation of roundoff error (Press and others, 1986).

Iterative methods involve generating a sequence of vectors

$$\mathbf{x^0} \rightarrow \mathbf{x^1} \rightarrow \mathbf{x^2} \rightarrow \cdots \tag{A-6}$$

which eventually converge to the correct solution x. The attractive feature of these methods is that the number of operations required for each step is comparable to multiplying the matrix of interest by a vector (Stoer and Bulirsch, 1980). Since we can ignore the zero entries when using an iterative scheme, a single iteration can be done quickly for a sparse matrix. The efficiency of the iterative methods depends, of course, on how quickly convergence is achieved. Because convergence may be slow, they are normally only applied to large sparse systems of equations.

One of the most commonly used methods is referred to as the *Gauss-Seidel* iteration (Ortega and Rheinboldt, 1970; Stoer and Bulirsch, 1980; Press and others, 1986). This method can be written as

$$a_{jj}\delta \ln C_j^{i+1} = b_j - \sum_{k<j} a_{jk} a \delta \ln C_k^{i+1} - \sum_{k>j} a_{jk} \delta \ln C_k^i \qquad (j = 1, 2, \ldots, N) \tag{A-7}$$

where the a_{ij} are the components of the Jacobian matrix, i and $i + 1$ refer to the iteration levels, and the $\delta \ln C_j$ are again the corrections to the logarithms of the concentrations of the primary species. In the Gauss-Seidel method, $\delta \ln C_j^{i+1}$ is taken as the solution of $\delta \ln C_j$. Note that in the Gauss-Seidel iteration, information from the $i + 1$ iteration is used as soon as it becomes available. In many cases it is possible to obtain faster rates of convergence by introducing a *relaxation parameter* ω. If $\delta \ln C_j^*$is the solution of the Gauss-Seidel iteration, then the value of $\delta \ln C_j^{i+1}$ is obtained from

$$\delta \ln C_j^{i+1} = \delta \ln C_j^i + \omega(\delta \ln C_j^* - \delta \ln C_j^i). \tag{A-8}$$

This is referred to as the SOR or *successive overrelaxation* method (Ortega and Rheinboldt, 1970; Press and others, 1986) which reduces to the Gauss-Seidel iteration when $\omega = 1$. When the SOR (or Gauss-Seidel) iteration is used to solve the set of linear equations that arise from the use of Newton's method (eq 43), the composite method is referred to as a *Newton-SOR* iteration, with Newton's method as the *primary* iteration and SOR as the *secondary* iteration (Ortega and Rheinboldt, 1970).

The ordered structure of the Jacobian matrices which arise in coupled reaction-transport problems suggest the use of *block iterative* procedures (Stoer and Bulirsch, 1980). These methods are based on a division of the matrix **A** into N partitions, each of which is a system of equations to be solved. One can think of the block iterative methods as a way of mixing iterative methods, which are suitable for large sparse matrices of the kind that arise from finite difference or finite element formulations and direct methods (for example, LU decomposition), which work best on smaller, dense matrices. The method employed in the code developed here is the *block SOR* method. When the relaxation parameter ω is taken as 1, the method reduces to the *block Gauss-Seidel* method which takes the form

$$\mathbf{A}_{jj}\delta \ln \mathbf{C}_j^{i+1} = \mathbf{b}_j - \sum_{k<j} \mathbf{A}_{jk}\delta \ln \mathbf{C}_k^{i+1} - \sum_{k>j} \mathbf{A}_{jk}\delta \ln \mathbf{C}_k^{i} \qquad (j = 1, 2, \ldots, N) \qquad \text{(A-9)}$$

where N is the number of partitions used. Note that the *block Gauss-Seidel* method becomes identical to the more familiar *Gauss-Seidel* method described above (Press and others, 1986) when the size of the partition is chosen to be 1. In this (trivial) case, the submatrices $\mathbf{A}_{ij}$ revert to the single entries a_{ij} in the Jacobian matrix. From eq (A-9), it is apparent that in order to solve for the vector $\delta \ln \mathbf{C}_j$, the diagonal submatrices (the $\mathbf{A}_{jj}$) must be non-singular so that they can be inverted at every iteration. By examining the structure of the Jacobian matrix in eq (A-5), it appears that the obvious way to proceed in the case of reaction-transport problems is to choose N in eq (A-9) (the number of partitions) as M, the number of grid points in the system. This implies that the size of each partition is N_c, the number of primary species in the system. At each iteration step, therefore, M systems of N_c linear equations need to be solved for reaction-transport problems. With the block iterative methods, it is possible to use LU decomposition on the relatively small ($N_c \times N_c$), dense submatrices corresponding to the reaction terms and an iterative procedure taking advantage of the sparseness of the global matrix **A**. The diagonal submatrices can be converted to the LU form so that only the back substitution step need be carried out at every iteration.

References

Aagaard, P., and Helgeson, H. C., 1982, Thermodynamic and kinetic constraints on reaction rates among minerals and aqueous solutions, I, Theoretical considerations: American Journal of Science, v. 282, p. 237–285.

Ague, J. J., and Brimhall, G. H., 1989, Geochemical modeling of steady state fluid flow and chemical reaction during supergene enrichment of porphyry copper deposits: Economic Geology, v. 84, p. 506–528.

Anderson, R. M., Langseth, M. G., and Sclater, J., 1977, The mechanisms of heat transfer through the floor of the Indian Ocean: Journal of Geophysical Research, v. 82, p. 3391–3409.

Aris, R., 1965, Prolegomena to the rational analysis of systems of chemical reactions: Archives of Rational Mechanics and Analysis, v. 19, p. 81–99.

Bahr, J. M., and Rubin, J., 1987, Direct comparison of kinetic and equilibrium formulations for solute transport affected by surface reactions: Water Resources Research, v. 23, p. 438–452.

Bear, J., 1972, Dynamics of Fluids in Porous Media: New York, American Elsevier, 764 p.

———— 1979, Hydraulics of Groundwater: New York, McGraw-Hill, 569 p.

Berman, R. G., 1988, Internally-consistent thermodynamic data for minerals in the system Na_2O-K_2O-CaO-MgO-FeO-Fe_2O_3 -Al_2O_3-SiO_2-TiO_2-H_2 O-CO_2: Journal of Petrology, v. 29, p. 445–522.

Berner, R. A., 1980, Early Diagenesis: A Theoretical Approach: Princeton, New Jersey, Princeton University Press, 241 p.

Bethke, C. M., 1985, A numerical model of compaction-driven groundwater flow and heat transfer and its application to the paleohydrology of intracratonic sedimentary basins: Journal of Geophysical Research, v. 90, p. 6817–6828.

———— 1986, Hydrologic constraints on the genesis of the Upper Mississippi Valley mineral district from Illinois basin brines: Economic Geology, v. 81, p. 233–249.

Bickle, M. J., and McKenzie, D., 1988, The transport of heat and matter by fluids during metamorphism: Contributions to Mineralogy and Petrology, v. 95, p. 384–392.

Bowen, R. M., 1968, On the stoichiometry of chemically reacting materials: Archives of Rational Mechanics and Analysis, v. 29, p. 114–124.

Bowers, T. S., and Taylor, H. P., Jr., 1985, An integrated chemical and stable-isotope model of the origin of midocean ridge hot spring systems: Journal of Geophysical Research, v. 90, p. 12,583–12,606.

Brace, W. F., 1984, Permeability of crystalline rocks: New in situ measurements: Journal of Geophysical Research, v. 89, p. 4327–4330.

Brimhall, G. H., Jr., 1980, Deep hypogene oxidation of porphyry copper potassium-silicate protore at Butte, Montana: A theoretical evaluation of the copper remobilization hypothesis: Economic Geology, v. 75, p. 384–409.

Brimhall, G. H., Jr., and Ghiorso, M. S., 1983, Origin and ore-forming consequences of the advanced argillic alteration process in hypogene environments by magmatic gas contamination of meteoric fluids: Economic Geology, v. 78, p. 73–90.

Bruges, E. A., Latto, B., and Ray, A. K., 1966, New correlations and tables of the coefficient of viscosity of water and steam up to 1000 bar and 1000°C: International Journal of Heat and Mass Transfer, v. 9, p. 465–480.

Bryant, S. L., Schechter, S. L., and Lake, L. W., 1987, Mineral sequences in precipitation/dissolution waves: American Institute of Chemical Engineering Journal, v. 33, p. 1271–1287.

Burch, T. E., Nagy, K. L., and Lasaga, A. C., 1993, Free energy dependence of albite dissolution kinetics at 80°C and pH 8.8: Chemical Geology, v. 105, p. 137–165.

Cathles, L. M., 1977, An analysis of the cooling of intrusives by ground water convection which includes boiling: Economic Geology, v. 72, p. 804–826.

———— 1981, Fluid flow and genesis of hydrothermal ore deposits, *in* Skinner, B. J. and Sims, P. K., editors, Economic Geology 75th Anniversary Volume: New Haven, Ct, Economic Geology Publications, p. 424–457.

———— 1983, An analysis of the hydrothermal system responsible for massive sulfide deposition in the Hokuroku Basin of Japan: Economic Geology Monograph 5, p. 439–487.

Chen, W., Ghaith, A., Park, A., and Ortoleva, P., 1990, Diagenesis through coupled processes: Modeling approach, self-organization, and implications for exploration, *in* Meshri, I. D., and Ortoleva, P., editors, Prediction of Reservoir Quality through Chemical Modeling: American Association of Petroleum Geologists Memoir 49, p. 103–130.

Cheng, P., 1978, Heat transfer in geothermal systems: Advances in Heat Transfer, v. 14, p. 1–105.

Clauser, C., 1992, Permeability of crystalline rocks: EOS, v. 73, p. 233.

Combarnous, M. A., and Bories, S. A., 1975, Hydrothermal convection in saturated porous media: Advances in Hydroscience, v. 10, p. 231–307.

Daus, A. D., and Frind, E. O., 1985, An alternating direction Galerkin technique for simulation of contaminant transport in complex groundwater systems: Water Resources Research, v. 21, p. 653–664.

Davis, E. E., Chapman, D. S., Forster, C. B., and Villinger, H., 1989, Heat-flow variations correlated with buried basement topography on the Juan de Fuca Ridge flank: Nature, v. 342, p. 533–537.

Donaldson, I. G., 1962, Temperature gradients in the upper layers of the Earth's crust due to convective water flows: Journal of Geophysical Research, v. 67, p. 3449–3459.

Elder, J. W., 1965, Physical processes in geothermal areas, *in* Lee, W. H. K., editor, Terrestrial Heat Flow: Geophysical Monograph Series, v. 8, p. 211–239.

———— 1967a, Transient convection in a porous medium: Journal of Fluid Mechanics, v. 27, p. 609–623.

———— 1967b, Steady free convection in a porous medium: Journal of Fluid Mechanics, v. 27, p. 29–48.

———— 1981, Geothermal Systems: Troy, Massachusetts, Academic, 508 p.

Fehn, U., and Cathles, L., 1986, The influence of plate movement on the evolution of hydrothermal convection cells in the oceanic crust: Tectonophysics, v. 125, p. 289–312.

Ferry, J. M., and Dipple, G. M., 1991, Fluid flow, mineral reactions, and metasomatism: Geology, v. 19, p. 211–214.

Fletcher, R. C., and Hoffman, A. W., 1974, Simple model of diffusion and combined diffusion-infiltration metasomatism, *in* Hofmann, A. W., Giletti, B. J., Yoder, H. S. and Yund, R. A., editors, Geochemical Transport and Kinetics: Carnegie Institute of Washington, p. 243–259.

Fournier, R. O., 1989, Geochemistry and dynamics of the Yellowstone National Park hydrothermal systems: Annual Reviews of Earth and Planetary Science, v. 17, p. 13–53.

Frind, E. O. and Germain, D., 1986, Simulation of contaminant plumes with large dispersive contrast: Evaluation of alternating direction Galerkin models: Water Resources Research, v. 22, p. 1857–1873.

Garven, Grant, 1989, A hydrogeologic model for the formation of the giant oil sands deposits of the Western Canada sedimentary basin: American Journal of Science, v. 289, p. 105–166.

Garven, Grant, and Freeze, R. A., 1984a, Theoretical analysis of the role of groundwater flow in the genesis of stratabound ore deposits: 1. Mathematical and numerical model: American Journal of Science, v. 284, p. 1085–1124.

———— 1984b, Theoretical analysis of the role of groundwater flow in the genesis of stratabound ore deposits: 2. Quantitative results: American Journal of Science, v. 284, p. 1125–1174.

Golub, G. H., and Van Loan, C. F., 1989, Matrix Computations: Baltimore, Maryland, Johns Hopkins Press, 642 p.

Helgeson, H. C., 1968, Evaluation of irreversible reactions in geochemical processes involving minerals and aqueous solutions-I. Thermodynamic relations: Geochimica et Cosmochimica Acta, v. 32, p. 853–877.

———— 1979, Mass transfer among minerals and hydrothermal solutions, *in* Barnes, H. L., editor, Geochemistry of Hydrothermal Ore Deposits: New York, John Wiley & Sons, p. 568–610.

Helgeson, H. C., Garrels, R. M., and MacKenzie, F. T., 1969, Evaluation of irreversible reactions in geochemical processes involving minerals and aqueous solutions-II. Applications: Geochimica et Cosmochimica Acta, v. 33, p. 455–482.

Helgeson, H. C., and Kirkham, D. H., 1974, Theoretical predictions of the thermodynamic behavior of aqueous electrolytes at high pressures and temperatures; I: Summary of the thermodynamic/electrostatic properties of the solvent: American Journal of Science, v. 274, p. 1089–1198.

Helgeson, H. C., Murphy, W. M., and Aagaard, P., 1984, Thermodynamic and kinetic constraints on reaction rates among minerals and aqueous solutions. II. Rate constants, effective surface area, and the hydrolysis of feldspar: Geochimica et Cosmochimica Acta, v. 48, p. 2405–2432.

Hoefner, M. L., and Fogler, H. S., 1988, Pore evolution and channel formation during flow and reaction in porous media: American Institute of Chemical Engineering Journal, v. 34, p. 45–54.

Hooyman, G. J., 1961, On thermodynamic coupling of chemical reactions: Washington, D.C., Proceeding of National Academy of Science, v. 47, p. 1169–1173.

Kee, R. J., and Petzold, L. R., Smooke, M. D., and Grcar, J. F., 1985, Implicit methods in combustion and chemical kinetics modeling, *in* Brackbill, J. U. and Cohen, B. I., editors, Multiple Time Scales: New York, Academic Press, p. 113–144.

Kerrick, D. M., Lasaga, A. C., and Raeburn, S. P., 1991, Kinetics of heterogeneous reactions, *in* Kerrick, D. M., editor, Contact Metamorphism: Reviews of Mineralogy, v. 26, p. 583–671.

Kirkner, D. J., and Reeves, H., 1988, Multicomponent mass transport with homogeneous and heterogeneous chemical reactions: Effect of chemistry on the choice of numerical algorithm. I. Theory: Water Resources Research, v. 24, p. 1719–1729.

Knapp, R. B., 1989, Spatial and temporal scales of local equilibrium in dynamic fluid-rock systems: Geochimica et Cosmochimica Acta, v. 53, p. 1955–1964.

Lapidus, L., and Pinder, G. F., 1982, Numerical Solution of Partial Differential Equations in Science and Engineering: New York, John Wiley & Sons, 677 p.

Lasaga, A. C., 1981, Rate laws in chemical reactions, *in* Lasaga, A. C., and Kirkpatrick, R. J., editors, Kinetics of Geochemical Processes: Reviews of Mineralogy, v. 8, p. 135–169.

———— 1984, Chemical kinetics of water-rock interactions: Journal of Geophysical Research, v. 89, p. 4009–4025.

———— 1986, Metamorphic reaction rate laws and development of isograds: Mineralogical Magazine, v. 50, p. 359–373.

———— 1989, Fluid flow and chemical reaction kinetics in metamorphic systems: a new simple model: Earth and Planetary Science Letters, v. 94, p. 417–424.

———— 1990, Atomic treatment of mineral-water surface reactions, *in* Hochella, M. F., Jr., and White, A. F., editors, Mineral-Water Interface Geochemistry: Reviews in Mineralogy, v. 23, p. 17–85.

Lasaga, A. C., and Rye, D. M., 1993, Fluid flow and chemical reaction kinetics in metamorphic systems: American Journal of Science, v. 293, p. 361–404.
Lassey, K. R., and Blattner, P., 1988, Kinetically controlled oxygen isotope exchange between fluid and rock in one-dimensional advective flow: Geochimica et Cosmochimica Acta, v. 52, p. 2169–2175.
Lichtner, P. C., 1985, Continuum model for simultaneous chemical reactions and mass transport in hydrothermal systems: Geochimica et Cosmochimica Acta, v. 49, p. 779–800.
———— 1988, The quasi-stationary state approximation to coupled mass transport and fluid-rock interaction in a porous medium: Geochimica et Cosmochimica Acta, v. 52, p. 143–165.
———— 1992, Time-space continuum description of fluid/rock interaction in permeable media: Water Resources Research, v. 28, p. 3135–3155.
———— 1993, Scaling properties of time-space kinetic mass transport equations and the local equilibrium limit: American Journal of Science, v. 293, p. 257–296.
Lichtner, P. C., and Biino, G. G., 1992, A first principles approach to supergene enrichment of a porphyry copper protore, I, Cu-Fe-S-H_2O subsystem: Geochimica et Cosmochimica Acta, v. 56, p. 3987–4013.
Liu, C. W., and Narasimhan, T. N., 1989a, Redox-controlled multiple-species reactive chemical transport, 1., Model development: Water Resources Research, v. 25, p. 869–882.
———— 1989b, Redox-controlled multiple-species reactive chemical transport, 2., Verification and application: Water Resources Research, v. 25, p. 883–910.
Lowell, R. P., 1991, Modeling continental and submarine hydrothermal systems: Reviews of Geophysics, v. 29, p. 457–476.
Lowell, R. P., Van Cappellen, P., and Germanovich, L. N., 1993, Silica precipitation in fractures and the evolution of permeability in hydrothermal upflow zones: Science, v. 260, p. 192–194.
Mangold, D. C., and Tsang, C., 1991, A summary of subsurface hydrological and hydrochemical models: Reviews of Geophysics, v. 29, p. 51–79.
Manning, C. E., and Bird, D. K., 1991, Porosity evolution and fluid flow in the basalts of the Skaergaard magma-hydrothermal system, East Greenland: American Journal of Science, v. 291, p. 201–257.
Marsily, G.de, 1986, Quantitative Hydrogeology: New York, Academic Press, 440 p.
Merino, E., Nahon, D., and Wang, Y., 1993, Kinetics and mass transfer of pseudomorphic replacement: Application to the replacement of parent minerals and kaolinite by Al, Fe, and Mn oxides during weathering: American Journal of Science, v. 293, p. 135–155.
Marsily, G.de, 1986, Quantitative Hydrogeology: New York, Academic Press, 440 p.
Merino, E., Nahon, D., and Wang, Y., 1993, Kinetics and mass transfer of pseudomorphic replacement: Application to the replacement of parent minerals and kaolinite by Al, Fe, and Mn oxides during weathering: American Journal of Science, v. 293, p. 135–155.
Miller, C. W., and Benson, L. V., 1983, Simulation of solute transport in a chemically reactive heterogeneous system: Model development and application: Water Resources Research, v. 19, p. 381–391.
Murphy, W. M., Oelkers, E. H., and Lichtner, P. C., 1989, Surface reaction versus diffusion control of mineral dissolution and growth rates in geochemical processes: Chemical Geology, v. 78, p. 357–380.
Nagy, K. L., Blum, A. E., and Lasaga, A. C., 1991, Dissolution and precipitation kinetics of kaolinite at 80°C and pH 3: The dependence on solution saturation state: American Journal of Science, v. 291, p. 649–686.
Nagy, K. L., and Lasaga, A. C., 1992, Dissolution and precipitation kinetics of gibbsite at 80°C and pH 3: The dependence on solution saturation state: Geochimica et Cosmochimica Acta, v. 56, p. 3093–3111.
Nagy, K. L., Steefel, C. I., Blum, A. E., and Lasaga, A. C., 1990, Dissolution and precipitation kinetics of kaolinite: Initial results at 80°C with application to porosity evolution in a sandstone, *in* Meshri, I. D., and Ortoleva, P., editors, Prediction of Reservoir Quality through Chemical Modeling: American Association of Petroleum Geologists Memoir 49, p. 85–101.
Narasimhan, T. N., and Witherspoon, P. A., 1976, An integrated finite differences method for analyzing fluid flow in porous media: Water Resources Research, v. 12, p. 57–64.
Norton, D., 1978, Sourcelines, source regions and pathlines for fluids in hydrothermal systems related to cooling plutons: Economic Geology, v. 73, p. 21–28.
———— 1984, A theory of hydrothermal systems: Annual Reviews of Earth and Planetary Science, v. 12, p. 155–177.

Norton, D., and Cathles, L. M., 1979, Thermal aspects of ore deposition, *in* Barnes, H. L., editor, Geochemistry of Hydrothermal Ore Deposits: New York, John Wiley & Sons, p. 611–631.

Norton, D., and Knapp, R., 1977, Transport phenomena in hydrothermal systems: the nature of porosity: American Journal of Science, v. 277, p. 913–936.

Norton, D., and Knight, J., 1977, Transport phenomena in hydrothermal systems: cooling plutons: American Journal of Science, v. 277, p. 937–981.

Norton, D., and Taylor, H. P., Jr., 1979, Quantitative simulation of the hydrothermal systems of crystallizing magmas on the basis of transport theory and oxygen isotope data: Skaergaard intrusion: Journal of Petrology, v. 20, p. 421–486.

Novak, C. F., Schechter, R. S., and Lake, L. W., 1989, Diffusion and solid dissolution/precipitation in permeable media: American Institute of Chemical Engineering Journal, v. 35, p. 1057–1072.

Ogata, A., and Banks, R. B., 1961, A solution of the differential equation of longitudinal dispersion in porous media: U.S. Geological Survey Professional Paper 411-A, p.

Ohmoto, H., and Lasaga, A. C., 1982, Kinetics of reactions between aqueous sulfates and sulfides in hydrothermal systems: Geochimica et Cosmochimica Acta, v. 46, p. 1727–1745.

Oran, E. S., and Boris, J. P., 1987, Numerical Simulation of Reactive Flow: New York, Elsevier, 601 p.

Ortega, J. M., and Rheinboldt, W. C., 1970, Iterative Solution of Nonlinear Equations in Several Variables: San Diego, California Academic Press, 572 p.

Ortoleva, P., Chadam, J., Merino, E., and Sen, A., 1987, Geochemical self-organization II: The reactive-infiltration instability: American Journal of Science, v. 287, p. 1008–1040.

Parkhurst, L. C., Thorstenson, D. C., and Plummer, L. N., 1980, PHREEQE-A computer program for geochemical calculations: U.S. Geological Survey Water Resources Investigations, p. 80–96.

Patankar, S. V., 1980, Numerical Heat Transfer and Fluid Flow: New York, Hemisphere Publishing, 197 p.

Patel, M. K., Cross, M., and Markatos, N. C., 1988, An assessment of flow oriented schemes for reducing 'false diffusion': International Journal of Numerical Methods in Engineering, v. 26, p. 2279–2304.

Peters, R. R., Klavetter, E. A., Hall, I. J., Blair, S. C., Heller, P. R., and Gee, G. W., 1984, Fracture and matrix hydrologic characteristics of tuffaceous materials from Yucca Mountain, Nye County, Nevada: Albuquerque, New Mexico, Sandia National Laboratory, Report SAND84-1471.

Phillips, O. M., 1991, Flow and reactions in permeable rocks: Cambridge, Cambridge University Press, 277 p.

Press, W. H., Flannery, B. P., Teukolsky, S. A., and Vetterling, W. T., 1986, Numerical Recipes: The Art of Scientific Computing: Cambridge, Cambridge University Press, 818 p.

Pruess, K., Wang, J. S. Y., and Tsang, Y. W., 1990, On thermohydrologic conditions near high-level nuclear wastes emplaced in partially saturated fractured tuff, 1, Simulation studies with explicit consideration of fracture effects: Water Resources Research, v. 26, p. 1235–1248.

Reed, M. H., 1982, Calculation of multicomponent chemical equilibria and reaction processes in systems involving minerals, gases, and an aqueous phase: Geochimica et Cosmochimica Acta, v. 46, p. 513–528.

———— 1983, Seawater-basalt reaction and the origin of greenstones and related ore deposits: Economic Geology, v. 78, p. 466–485.

Reeves, H., and Kirkner, D. J., 1988, Multicomponent mass transport with homgenous and heterogeneous chemical reactions: Effect of chemistry on the choice of numerical algorithm. 2. Numerical results: Water Resources Research, v. 24, p. 1730–1739.

Rheinboldt, W. C., 1974, Methods for Solving Systems of Nonlinear Equations: Philadelphia, Society for Industrial and Applied Mathematics, 104 p.

Ribando, R. J., and Torrance, K. E., 1976, Natural convection in a porous medium: Effects of confinement, variable permeability, and thermal boundary conditions: Journal of Heat Transfer, v. 98, p. 42–48.

Rimstidt, J. D., and Barnes, H. L., 1980, The kinetics of silica-water reactions: Geochimica et Cosmochimica Acta, v. 44, p. 1683–1699.

Rubin, J., 1983, Transport of reacting solutes in porous media: relation between mathematical nature of problem formulation and chemical nature of reactions: Water Resources Research, v. 19, p. 1231–1252.

Sanford, W. E., and Konikow, L. F., 1989, Simulation of calcite dissolution and porosity changes in saltwater mixing zones in coastal aquifers: Water Resources Research, v. 25, p. 655–667.

Schechter, R. S., Bryant, S. L., and Lake, L. W., 1987, Isotherm-free chromatography: propagation of precipitation/dissolution waves: Chemical Engineering Communications, v. 58, p. 353–376.

Scott, R. B., Spengler, R. W., Diehl, S., Lappin, A. R., and Chornack, M. P., 1982, Geologic character of tuffs in the unsaturated zone at Yucca Mountain, Southern Nevada, *in* Mercer, J., Rao, P. S., and Marine, I. W., editors, Role of the Unsaturated Zone in Radioactive and Hazardous Waste Disposal: Ann Arbor, Michigan, Ann Arbor Science, p. 289–335.

Sevougian, S. D., Schechter, R. S., and Lake, L. W., 1993, The effect of partial local equilibrium on the propagation of precipitation/dissolution waves: Industrial and Engineering Chemistry Research, v. 32, p. 2281–2304.

Snow, D. T., 1970, The frequency and apertures of fractures in rock: International Journal of Rock Mechanics Mineral Science, v. 7, p. 23–40.

Steefel, C. I., ms, 1992, Coupled fluid flow and chemical reaction: Model development and application to water-rock interaction: Ph.D. thesis, Yale University, New Haven, Connecticut, 234 p.

Steefel, C. I., and Lasaga, A. C., 1990, Evolution of dissolution patterns: Permeability change due to coupled flow and reaction, *in* Melchior, D. C. and Bassett, R. L., editors, Chemical Modeling in Aqueous Systems II: American Chemical Society Symposium Series, no. 416, p. 212–225.

———— 1992, Putting transport into water-rock interaction models: Geology, v. 20, p. 680–684.

Steefel, C. I., and Van Cappellen, P., 1990, A new kinetic approach to modeling water-rock interaction: The role of nucleation, precursors, and Ostwald ripening: Geochimica et Cosmochimica Acta, v. 54, p. 2657–2677.

Stoer, J., and Bulirsch, R., 1980, Introduction to Numerical Analysis: New York, Springer-Verlag, 609 p.

Sverjensky, D. A., 1984, Oil field brines as ore-forming solutions: Economic Geology, v. 79, p. 23–37.

Sverjensky, D. A., Hemley, J. J., and D'Angelo, W. M., 1991, Thermodynamic assessment of hydrothermal alkali feldspar-mica-aluminosilicate equilibria: Geochimica et Cosmochimica Acta, v. 55, p. 989–1004.

Thompson, J. B., 1959, Local equilibrium in metasomatic processes, *in* Abelson, P. H., editor, Researches in Geochemistry: New York, John Wiley & Sons, p. 427–457.

Truesdell, A. H., and Fournier, R. O., 1976, Conditions in the deeper parts of the hot spring systems of Yellowstone National Park, Wyoming: U.S. Geological Survey Open File Report 75–428, 29 p.

Turcotte, D. L., and Schubert, G., 1982, Geodynamics: Applications of Continuum Physics to Geologic Problems: New York, John Wiley & Sons, 450 p.

Van Cappellen, P., and Berner, R. A., 1991, Fluorapatite crystal growth from modified seawater solutions: Geochimica et Cosmochimica Acta, v. 55, p. 1219–1234.

Van Zeggeren, F., and Storey, S. H., 1970, The Computation of Chemical Equilibria: Cambridge, Cambridge University Press, 176 p.

Walsh, M. P., Bryant, S. L., Schecter, R. S., and Lake, L. W., 1984, Precipitation and dissolution of solids attending flow through porous media: American Institute of Chemical Engineering Journal, v. 30, p. 317–327.

Wells, J. T., and Ghiorso, M. S., 1991, Coupled fluid flow and reaction in mid-ocean ridge hydrothermal systems: The behavior of silica: Geochimica et Cosmochimica Acta, v. 55, p. 2467–2481.

White, D. E., Muffler, L. J. P., and Truesdell, A. A., 1971, Vapor-dominated hydrothermal systems as compared to hot-water systems: Economic Geology, v. 66, p. 75–97.

Wilson, E. N., Hardie, L. A., and Phillips, O. M., 1990, Dolomitization front geometry, fluid flow patterns and the origin of massive dolomite: the Triassic Latemar buildup: American Journal of Science, v. 290, p. 741–796.

Wolery, T. J., 1983, EQ3NR, a computer program for geochemical aqueous speciation-solubility calculations: Users guide and documentation: Lawrence Livermore Laboratory URCL-53414.

Wolery, T. J., Jackson, K. J., Bourcier, W. L., Bruton, C. J., Viani, B. E., Knauss, K. G., and Delany, J. M., 1990, Current status of the EQ3/6 software package for geochemical modeling, *in* Melchior, D. C. and Bassett, R. L., editors, Chemical Modeling in Aqueous Systems II: American Chemical Society Symposium Series, no. 416, p. 104–116.

Wood, J. R., and Hewett, T. A., 1982, Fluid convection and mass transfer in porous limestones: A theoretical model: Geochimica et Cosmochimica Acta, v. 46, p. 1707–1713.

Yeh, G. T., and Tripathi, V. S., 1989, A critical evaluation of recent developments in hydrogeochemical transport models of reactive multichemical components: Water Resources Research, v. 25, p. 93–108.

———— 1991, A model for simulating transport of reactive multispecies components: Model development and demonstration: Water Resources Research, v. 27, p. 3075–3094.